

Entrainment in Trouble: Cool Cloud Acceleration and Destruction in Hot Supernova-Driven Galactic Winds

Dong Zhang^{1,2,3*}, Todd A. Thompson^{2,3}, Eliot Quataert⁴ and Norman Murray^{5†}

¹*Department of Astronomy, University of Virginia, 530 McCormick Road, Charlottesville, VA 22904, USA*

²*Department of Astronomy, The Ohio State University, 140 West 18th Avenue, Columbus, OH 43210, USA*

³*Center for Cosmology & Astro-Particle Physics, The Ohio State University, Columbus, Ohio 43210, USA*

⁴*Astronomy Department & Theoretical Astrophysics Center, 501 Campbell Hall, University of California, Berkeley, CA 94720, USA*

⁵*Canadian Institute for Theoretical Astrophysics, 60 St. George Street, University of Toronto, Toronto, ON M5S 3H8, Canada*

16 October 2018

ABSTRACT

Efficient thermalization of overlapping supernovae within star-forming galaxies may produce a supernova-heated fluid that drives galactic winds. For fiducial assumptions about the timescale for cloud shredding from high-resolution simulations (which neglect magnetic fields) we show that cool clouds with temperature from $T_c \sim 10^2 - 10^4$ K seen in emission and absorption in galactic winds cannot be accelerated to observed velocities by the ram pressure of a hot wind. Taking into account both the radial structure of the hot flow and gravity, we show that this conclusion holds over a wide range of galaxy, cloud, and hot wind properties. This finding calls into question the prevailing picture whereby the cool atomic gas seen in galactic winds is entrained and accelerated by the hot flow. Given these difficulties with ram pressure acceleration, we discuss alternative models for the origin of high velocity cool gas outflows. Another possibility is that magnetic fields in cool clouds are sufficiently important that they prolong the cloud’s life. For $T_c = 10^3$ K and 10^4 K clouds, we show that if conductive evaporation can be neglected, the cloud shredding timescale must be ~ 15 and 5 times longer, respectively, than the values from hydrodynamical simulations in order for cool cloud velocities to reach those seen in observations.

Key words: galaxies: evolution — galaxies: formation — galaxies: fundamental parameters — galaxies: starburst — X-rays: galaxies

1 INTRODUCTION

Galactic winds are ubiquitous and important in rapidly star-forming galaxies. They are a primary source of metals in the intergalactic medium and affect the chemical evolution of galaxies (e.g., Dekel & Silk 1986; Aguirre et al. 2001; Finlator & Davé 2008; Peeples & Shankar 2011).

Several mechanisms have been proposed for launching galaxy-scale outflows. Among them, the very hot wind created by supernova (SN) energy injection is widely used in the literature. Chevalier & Clegg (1985) (hereafter CC85) developed a one-dimensional model for SN-driven winds with two controlling parameters: the thermalization efficiency with which SN-injected energy is converted into thermal energy, and the mass-loading efficiency, i.e., the ratio of the hot gas mass loss rate (\dot{M}_{hot}) to the host galaxy star formation rate (SFR): $\beta = \dot{M}_{\text{hot}}/\text{SFR}$. These two parameters are difficult to

determine observationally. For example, observational constraints on β have been determined for only a few galaxies, e.g., NGC 1569 (Martin 2002) and M82 (Strickland & Heckman 2009).

In Zhang et al. (2014) we derived a general constraint on β across a wide range of galaxies from dwarf starbursts to ultra-luminous infrared galaxies (ULIRGs) using the observed linear relation between the X-ray luminosity (L_X) and SFR (e.g., Mineo et al. 2012; Lehmer et al. 2010; Mineo et al. 2014). In contrast with the observations, the CC85 model predicts $L_X \propto \text{SFR}^2$ for the hot wind fluid if β is a constant. Thus the observed L_X –SFR relation can be used to constrain the hot wind. By combining the CC85 model with a band-dependent calculation of the X-ray emission and comparing with recent determinations of the L_X –SFR relation (Mineo et al. 2014) we showed that $\beta \lesssim 1$ for SFR $\gtrsim 10 M_\odot \text{ yr}^{-1}$. Larger values of β would overproduce X-rays.

This constraint on the hot wind outflow rate implies that the CC85 model alone cannot explain the $\beta \sim 1 - 10$ required by integrated constraints on stellar feedback models

* E-mail: dz7g@virginia.edu

† Canada Research Chair in Astrophysics

in a cosmological context (i.e., Oppenheimer & Davé 2006, 2008; Finlator & Davé 2008; Bower et al. 2012; Puchwein & Springel 2013). However, galactic winds are known to be multi-phase, with clear evidence for neutral atomic and ionized gas in emission and absorption from multi-wavelength observations. For example, Na I D absorption-line surveys provide the kinematics of neutral atomic outflows in local starbursts and high- z star-forming galaxies (e.g., Heckman et al. 2000; Rupke et al. 2002, 2005a,b,c; Schwartz & Martin 2004; Martin 2005; Weiner et al. 2009; Erb et al. 2012; Kornei et al. 2013). Emission lines such as H α , N II, O II, OIII have also been used to probe cool outflowing gas in star-forming galaxies (see Veilleux et al. 2005 and reference therein). In addition, both cool and warm molecular gas are detected in outflows in some local and high- z galaxies (e.g., Sakamoto et al. 1999; Walter et al. 2002; Veilleux et al. 2009; Fischer et al. 2010; Sturm et al. 2011; Bolatto et al. 2013; Ciccone et al. 2014). Obvious questions are whether or not the cool clouds are the dominant gas mass reservoir in the surrounding hot wind, whether or not they are accelerated by the ram pressure of the hot wind to the velocities seen, and whether or not the clouds survive the process of acceleration to both large physical scales and large velocities in order to match the spatially-resolved morphology seen in some local systems (e.g., Heckman et al. 1990; Heckman et al. 2000; Martin 2005; Veilleux et al. 2005; Leroy et al. 2015). These same issues are directly connected to the recent finding of a potentially large cool gas reservoir on 100 kpc scales in the halos of $z \sim 0$ galaxies (e.g., Werk et al. 2014).

In this paper we seek general constraints on the ram pressure acceleration (RPA) of cool clouds over a broad parameter space that includes the hot wind properties (thermalization and mass-loading efficiencies), cool cloud properties (density, column density, and temperature), and galaxy properties (star formation rate, velocity dispersion of the host gravitational potential) from dwarf starbursts to ULIRGs. Our primary goal is to assess and quantify cloud survival and acceleration in hot winds for comparison with observations of cold, cool, and warm molecular and atomic gas from $\sim 10^2 - 10^4$ K.¹

A number of studies have discussed the interaction between cool clouds and the surrounding hot outflow in rapidly star-forming galaxies. On the observational side, the thermal soft X-ray emission shows that the hot ionized interstellar stellar medium (ISM) has a temperature of $T_X \sim 0.2 - 0.8$ keV in all kinds of starburst galaxies from dwarfs to ULIRGs (Martin 1999; Heckman et al. 2000; Huo et al. 2004; Grimes et al. 2005). The hot gas would be expected to accelerate cool clouds to a maximum terminal velocity of $\sqrt{3}c_s \simeq 450(k_B T_X / 0.7\text{keV})^{1/2}$ km s⁻¹, similar to the average velocities of cool outflows (Heckman et al. 2000; Rupke et al. 2002, 2005a,c; Martin 2005; Weiner et al. 2009). On the other hand, cool gas with very high velocities above 500 km s⁻¹ is also observed in some LIRGs and ULIRGs, which *prima facie* cannot be explained by acceleration via ram pressure of the wind that emits in soft X-rays. Thus, the very high velocity cool gas is expected to be explained

by the RPA of a much hotter wind fluid associated with the diffuse hard X-ray emission. Recent observations of diffuse hard X-ray emission in M82 imply the existence of gas with $T > 10^7$ K (e.g., Strickland et al. 2004a; Strickland & Heckman 2009), which in the CC85 model would be associated with a hot wind with terminal velocity of $\sim 1000 - 2000$ km s⁻¹. The H α filaments in M82 with velocity of $V_{H\alpha} \sim 600$ km s⁻¹ (McKeith et al. 1995; Shopbell & Bland-Hawthorn 1998) are also proposed to be produced by RPA of cool clouds within the hot wind (e.g., Cooper et al. 2008, 2009).

On the theoretical side, numerical simulations have explored both the galaxy-scale ram pressure acceleration and production of cool clouds by a hot flow (e.g., Strickland & Stevens 2000; Cooper et al. 2008; Fujita et al. 2009; Hopkins et al. 2012) and the survival of individual (or a set of) ram pressure accelerated clouds at high numerical resolution (e.g., Klein et al. 1994; Schiano et al. 1995; Vietri et al. 1997; Cooper et al. 2009; Heckman et al. 2000; Nakamura et al. 2006; Orlando et al. 2008; Jun et al. 1996; Poludnenko et al. 2002; Pittard et al. 2005; Alúzar et al. 2012). The galaxy-scale simulations of winds in general have coarse spatial resolution compared to what would be required to fully resolve conductive evaporation, magnetic draping, and the Rayleigh-Taylor and Kelvin-Helmholtz instabilities. Most are also tuned to one particular system (e.g., M82) and prescribe an unrealistic uniform starburst ISM as the starting condition (although, see Cooper et al. 2008; Hopkins et al. 2012). On the other hand, although the high-resolution simulations capture much of the very small-scale physics of the clouds and their evaporation or destruction, they generically do not vary the properties of the hot wind widely or explore the evolution of the wind properties with radius as the cloud is accelerated. They also do not ask about the global effects of gravity relative to the ram pressure force, or conduct parameter studies across a wide variety of cloud properties.

In this paper, we model the dynamics of cool clouds in hot winds, varying the parameters of the problem, and tracking the dynamics of the clouds themselves, informed by the high-resolution simulations from the literature. We seek general constraints on the RPA scenario by comparing velocities, column densities, and temperatures with observations. Some quantities are given in Table 1. In Section 2 we first review the hot wind solutions of CC85. We then present analytic constraints on various timescales of clouds in the hot flow, including their destruction by hydrodynamical instabilities (in particular the Kelvin-Helmholtz instability), and the acceleration timescale. We highlight the fact that acceleration timescale of the cloud is always longer than the timescale for cloud hydrodynamical instabilities, and thus the hot flow cannot accelerate cool clouds to its asymptotic velocity. We also compare the gravitational force with the ram pressure force, deriving a general Eddington-like limit as a function of cloud and host galaxy properties, which strongly constraints the initial column densities of accelerated clouds. In Section 3 we calculate cloud acceleration numerically in a spherically-symmetric model, parameterizing destruction processes and following the evolution of the cloud as it is accelerated, and as the hot wind (its density, temperature and Mach number) evolves as a function of radius. Note that a complicating factor is that the cloud destruction timescale by instabilities remains uncertain, and is a function of both the radiative properties of the cloud

¹ We refer to all of these clouds as “cool” throughout this paper unless we wish to make distinction between clouds that would be expected to be largely molecular, neutral atomic, or ionized.

and its magnetization as it is crushed and accelerated by the hot flow. Recent magnetohydrodynamic simulations of isothermal clouds suggest much longer cloud lifetimes than indicated by pure hydrodynamical simulations (McCourt et al. 2015). For this reason, in Section 3 we also provide additional discussion of cloud dynamics when the cloud shredding timescale is taken as a free parameter, and we derive the critical value of this timescale such that clouds are accelerated to high velocities as a guide for future simulations and comparing with observations. In Section 4 we combine the X-ray model in Zhang et al. (2014) with the RPA model for case studies of individual systems. Conclusions are presented in Section 5. We also discuss the impacts of other model parameters and other possible wind driving mechanisms.

2 ANALYTIC CONSTRAINTS

We briefly summarize the CC85 model in this section. For more details see Zhang et al. (2014). Inside the radius of the starburst region $r \leq R$ the total energy and mass input into the hot wind are \dot{E}_{hot} and \dot{M}_{hot} and the volumetric energy and mass input rates are assumed to be constant. The flow outside the starburst region $r > R$ is assumed to be adiabatic. Under these assumptions, the Mach number $M = 0$ at $r = 0$, and $M = 1$ at $r = R$. The two controlling dimensionless parameters of the problem, the thermalization efficiency α and the hot gas mass-loading efficiency β are given by

$$\dot{E}_{\text{hot}} = \alpha \epsilon_0 \nu_0 \text{SFR}, \quad (1)$$

$$\dot{M}_{\text{hot}} = \beta \text{SFR}, \quad (2)$$

where $\epsilon_0 = 10^{51}$ ergs and $\nu_0 = (100 M_{\odot})^{-1}$ are the normalization values of the energy injected by an individual SN and the number of SNe per unit mass of star formation respectively. The temperature T , density n and velocity V_{hot} of the hot wind outflow are (see Zhang et al. 2014)

$$T(r) = 6.1 \times 10^7 \text{ K } \mu \left(\frac{\alpha}{\beta} \right) \left[\frac{P_*(r_*)}{\rho_*(r_*)} \right] \quad (3)$$

$$n(r) = 14 \text{ cm}^{-3} \alpha^{-1/2} \beta^{3/2} \mu^{-1} R_{200\text{pc}}^{-2} \rho_*(r_*) \text{SFR}_1 \quad (4)$$

$$V_{\text{hot}}(r) = 710 \text{ km s}^{-1} \alpha^{1/2} \beta^{-1/2} u_*(r_*), \quad (5)$$

where $R_{200\text{pc}} = R/(200 \text{ pc})$ is the wind launching radius in the host starburst, u_* , ρ_* and P_* are the dimensionless velocity, density and pressure as functions of the dimensionless radius $r_* = r/R$, and $\mu \approx 0.61$ is the mean molecular weight for solar abundance.

2.1 Initial Clouds

The dynamical timescale of the hot wind at radius r is

$$t_{\text{dyn}} \approx \frac{r}{V_{\text{hot}}} \approx 2.8 \times 10^5 \text{ yr } u_*^{-1} r_* \alpha^{-1/2} \beta^{1/2} R_{200\text{pc}}. \quad (6)$$

The cooling timescale is

$$t_{\text{cool}} \approx \varepsilon_{\text{heat}} / (n_e^{\text{hot}} n_{\text{H}}^{\text{hot}} \Lambda_{\text{N}}), \quad (7)$$

where $\varepsilon_{\text{heat}} \approx \rho \left(\frac{1}{2} V_{\text{hot}}^2 + \frac{c_s^2}{\gamma-1} \right) = \rho_* \dot{E}^{1/2} \dot{M}^{1/2} / R^2$ is the total energy of the flow, n_e^{hot} and $n_{\text{H}}^{\text{hot}}$ are the electron and

hydrogen density in the hot flow, and Λ_{N} is the emissivity of the flow. In Zhang et al. (2014) we showed that the criterion for an adiabatic hot wind flow with $t_{\text{cool}} \geq t_{\text{dyn}}$ at $r = R$ implies an upper limit on β of

$$\beta \leq 6.6 \alpha^{3/5} R_{200\text{pc}}^{2/5} \text{SFR}_1^{-2/5} \left(\frac{\Lambda_{\text{brems}}^{\text{H}}}{\Lambda_{\text{N}}} \right)^{2/5}, \quad (8)$$

where $\text{SFR}_1 = \text{SFR}/10 M_{\odot} \text{ yr}^{-1}$, and the bremsstrahlung emission $\Lambda_{\text{brems}}^{\text{H}}$ is used to estimate the lower limit for the cooling rate Λ_{N} , where Λ_{N} is calculated by the full SPEX package, assuming collisional ionization equilibrium and solar abundance (version 2.03.03, see Zhang et al. 2014, also Schure et al. 2009). Thus, the mass loading efficiency cannot be higher than given by equation (8) at $r = R$ or the system becomes radiative and the adiabatic solution for $r > R$ given by CC85 is invalidated (see Wang 1995; Silich et al. 2003, 2004; Thompson et al. 2016).

Strickland & Heckman (2009) showed that for an axisymmetric disklike starburst, there is a spherical starburst CC85 model with an equivalent radius R that can provide a good approximation in describing the hot wind solution in a disk-like starburst. The equivalent radius R in general is smaller than the radius of the star forming disk region R_d . In the following sections we first take a fiducial value of $R = 200 \text{ pc}$ as the equivalent radius of galaxies for simplicity. Different radii are explored below.

It is believed that the pressure of the hot wind fluid will entrain cool gas clouds from the ISM (e.g., Veilleux et al. 2009). In general, we expect the ISM of rapidly star-forming galaxies to be highly turbulent, with a broad log-normal distribution of densities and column densities and with a multi-phase medium. In order to explore constraints on the survival and dynamics of clouds, we first need to specify their properties. There are several parameters in our model for clouds: the temperature in the cloud T_c , the initial density and column density of the cloud n_{H}^i and N_{H}^i , and the starting position (launching radius) of the cloud r_0 . For simplicity, in our analytic estimates below and in Section 3, we consider isothermal clouds with $T_c = 10^2$, 10^3 , or 10^4 K as might be appropriate for molecular, neutral atomic, and ionized gas, respectively. Also, we consider clouds initially at radii $r \geq R$, and take $r_0 = R$, $2R$ and $3R$. In general the parameters are scaled in terms of fiducial values $T_{c,3} = T_c/10^3 \text{ K}$, $N_{\text{H}}^i = 10^{21} N_{\text{H},21}^i \text{ cm}^{-2}$, and $n_{\text{H}}^i = 10^3 n_{\text{H},3}^i \text{ cm}^{-3}$.

Given these sets of parameters for the cool clouds, we now estimate the timescales that describe their dynamics and survival in a hot CC85-like flow, including the timescales for cloud crushing, expansion, acceleration, evaporation, and hydrodynamical instability (e.g., the Kelvin-Helmholz and Rayleigh-Taylor timescales). The pressure in the cloud is

$$P_c = 1.4 \times 10^{-10} \text{ dynes cm}^{-2} n_{\text{H},3}^i T_{c,3} \quad (9)$$

The pressure in the hot wind is $P_{\text{hot}} = P_{\text{th}} + P_{\text{ram}}$, where P_{th} is the thermal pressure $k_B \rho_{\text{hot}} T_{\text{hot}} / (\mu m_{\text{H}})$, and the ram pressure of the hot wind $P_{\text{ram}} = \rho_{\text{hot}} V_{\text{hot}}^2$ is given by

$$P_{\text{ram}} = 1.2 \times 10^{-7} \text{ dynes cm}^{-2} \rho_0 u_0^2 \alpha^{1/2} \beta^{1/2} R_{200\text{pc}}^{-2} \text{SFR}_1, \quad (10)$$

where the dimensionless velocity u_0 , density ρ_0 are functions of radius (see Table 2). Here u_0 , ρ_0 and P_0 are u_* , ρ_* and P_* (see equations 3, 4, 5) evaluated at $r_* = r_0$, respectively. Since the hot wind is supersonic (Mach number $M_{\text{h}} \gg 1$ for

Notation	Definition	Section/Eq.
α	dimensionless thermalization efficiency	Section 2, eq.(1)
β	dimensionless mass-loading efficiency	Section 2, eq.(2)
R	starburst region	Section 2, eq.(4)
SFR	star formation rate in the galaxy	Section 2, eq.(4)
t_{dyn}	dynamical timescale of the hot flow	Section 2.1, eq.(6)
t_{cool}	cooling timescale of the hot flow	Section 2.1, eq.(7)
T_c	temperature of the cloud	Section 2.1, eq.(9)
n_{H}^i	initial hydrogen number density of the cloud	Section 2.1, eq.(9)
r_0	starting position of the cloud	Section 2.1
ρ_0, u_0, P_0	dimensionless velocity, density and pressure of the hot wind at r_0	Section 2.1, eq.(10)
t_{cc}	crushing timescale of the cloud	Section 2.1, eq.(11)
N_{H}^i	initial hydrogen column density of the cloud	Section 2.1, eq.(11)
R_c	radius of the cloud	Section 2.1, eq.(11)
t_{expan}	expansion timescale of the cloud	Section 2.1, eq.(12)
t_{acc}	acceleration timescale of the cloud	Section 2.1, eq.(14)
M_{h}	Mach number of the hot flow around cloud	Section 2.2, eq.(17)
t_{sh}	shredding timescale of the cloud	Section 2.2, eq.(18)
κ	parameter in the cloud shredding timescale	Section 2.2, eq.(18)
V_c^{sh}	maximum velocity of the cloud estimated by t_{sh}	Section 2.2, eq.(20)
t_{evap}	evaporation timescale of the cloud	Section 2.2, eq.(23)
V_c^{evap}	maximum velocity of the cloud estimated by t_{evap}	Section 2.2, eq.(25)
σ	velocity dispersion of the galaxy	Section 2.3, eq.(27)
n_{H}^c	hydrogen number density of cloud at pressure equilibrium with hot flow	Section 2.3, eq.(30)
N_{H}^c	hydrogen column density of cloud at pressure equilibrium with hot flow	Section 2.3, eq.(31)
$R_c^{\parallel}, R_c^{\perp}$	cloud radius parallel and perpendicular to the hot flow	Section 2.3, eq.(31)
ξ	$R_c^{\parallel}/R_c^{\perp}$	Section 2.3, eq.(31)
κ_{crit}	critical value of κ that gives $t_{\text{sh}} \sim t_{\text{acc}}$	Section 3.2, eq.(39)

Table 1. Notations and definitions of some quantities in this paper.

Properties of CC85 Wind Solutions				
	Eq.	$r_{0,*} = 1$	$r_{0,*} = 2$	$r_{0,*} = 3$
u_0		0.71	1.26	1.33
ρ_0		0.11	1.58e-2	6.64e-3
P_0		3.37e-2	1.27e-3	3.02e-4
M_{h}		1.0	3.44	4.84
$(1 + M_{\text{h}})^{-1/6} \rho_0^{-1/2} u_0^{-1} P_0^{-1/2}$	eq. (18)	20.4	137.8	395.3
$(1 + M_{\text{h}})^{1/3} P_0 \rho_0^{-1}$	eq. (19)	0.38	0.13	8.19e-2
$(1 + M_{\text{h}})^{-1/3} P_0^{-1}$	eq. (21)	23.6	477.7	1840
$(1 + M_{\text{h}})^{-1/3} M_{\text{h}}^{-1/2} P_0^{-3/4} u_0^{-1} \rho_0^{-1/4}$	eq. (23)	24.6	108.7	290.0
$(1 + M_{\text{h}})^{4/9} M_{\text{h}}^{2/3} P_0 \rho_0^{-1}$	eq. (24)	0.41	0.36	0.28
$M_{\text{h}}^{-1/2} (1 + M_{\text{h}})^{-1/3} P_0^{-3/4} u_0 \rho_0^{3/4}$	eq. (25)	1.39	2.73	3.41
$M_{\text{h}}^{-1} (1 + M_{\text{h}})^{-2/3} P_0^{-3/2} \rho_0^{1/2}$	eq. (26)	34.1	297.0	990.5
$(1 + M_{\text{h}})^{2/3} M_{\text{h}} (u_0/r_{0,*}) P_0^{3/2} \rho_0^{-3/2}$	eq. (29)	0.18	0.14	6.75e-2
$(1 + M_{\text{h}})^4 M_{\text{h}}^{-8} \rho_0 u_0^{-1}$	eq. (32)	2.52	2.47e-4	1.93e-5
$(1 + M_{\text{h}})^{-2/3} M_{\text{h}} u_0^{1/2} P_0^{-1/6}$	eq. (33)	0.93	4.35	6.65
$(1 + M_{\text{h}})^{-2/3} P_0^{-2/3}$	eq. (34)	6.04	31.5	68.5
$(1 + M_{\text{h}})^{1/6} P_0^{1/2} \rho_0^{-1/2}$	eq. (39)	0.61	0.36	0.29

Table 2. Here $r_{0,*} = r_0/R$, where r_0 is the the starting position of the cloud.

$r > R$), we have $P_{\text{ram}} \gg P_{\text{h}}$ and $P_{\text{hot}} \simeq P_{\text{ram}}$. If $P_{\text{ram}} > P_c$, a shock will be driven into the cool clouds on a cloud crushing time when the hot wind overtakes the cool cloud, where the crushing time is defined as the time needed for the shock to cross the cloud:

$$t_{\text{cc}} \approx \frac{R_c}{v_s} \approx \frac{R_c}{V_{\text{hot}}} \left(\frac{\rho_c}{\rho_{\text{hot}}} \right)^{1/2}$$

$$\approx 2.2 \times 10^3 \text{ yr } \rho_0^{-1/2} u_0^{-1} \alpha^{-1/4} \beta^{-1/4} \times (n_{\text{H},3}^i)^{-1/2} N_{\text{H},21}^i R_{200\text{pc}} \text{SFR}_1^{-1/2}, \quad (11)$$

and the shock velocity v_s is estimated as $v_s = (P_{\text{ram}}/\rho_c)^{1/2}$ (Klein et al. 1994; Murray et al. 2007). On the other hand, if $P_{\text{ram}} < P_c$, the cool gas cannot be pressure confined by the hot wind, and it will expand at its sound speed until

the cloud reaches pressure equilibrium with the surrounding medium. Thus, the expansion timescale for pressure equilibrium is

$$\begin{aligned} t_{\text{expan}} &\approx R_c \sqrt{\frac{m_{\text{H}}}{k_B T_c}} \\ &\approx 5.5 \times 10^4 \text{ yr } N_{\text{H},22}^i (n_{\text{H},3}^i)^{-1} T_{c,3}^{-1/2}. \end{aligned} \quad (12)$$

The initial acceleration timescale of the cloud, i.e., the time for the cloud to become comoving with the hot wind flow is of order ²

$$\begin{aligned} t_{\text{acc}} &\approx \frac{4R_c}{3V_{\text{hot}}} \left(\frac{\rho_c}{\rho_{\text{hot}}} \right) \\ &\approx 3.0 \times 10^4 \text{ yr } (\rho_0^{-1} u_0^{-1}) \beta^{-1} N_{\text{H},21}^i R_{200\text{pc}}^2 \text{SFR}_1^{-1} \end{aligned} \quad (14)$$

Comparing equations (11) and (14), we have that for

$$\beta \leq 32 \rho_0^{-2/3} \alpha^{1/3} (n_{\text{H},3}^i)^{2/3} R_{200\text{pc}}^{4/3} \text{SFR}_1^{-2/3} \quad (15)$$

the crushing time is less than the acceleration time $t_{\text{cc}} \leq t_{\text{acc}}$ with $P_{\text{ram}} > P_c$. Similarly, by comparing equations (12) and (14), we find that for

$$\beta \leq 0.55 (\rho_0^{-1} u_0^{-1}) R_{200\text{pc}}^2 n_{\text{H},3}^i T_{c,3}^{1/2} \text{SFR}_1^{-1}, \quad (16)$$

$t_{\text{expan}} \leq t_{\text{acc}}$ with $P_{\text{ram}} < P_c$. Note that we have treated the cloud as isothermal, because the shocked gas inside the cloud quickly cools to 10^4 K or below on a timescale of ~ 100 yr, much shorter than the timescales we consider below (Murray et al. 2007; Fujita et al. 2009). We take the temperature of the cool cloud as a constant, but always include the T_c scaling.

In Figure 1 we show timescale constraints as a function of the mass loading efficiency β and SFR for clouds with temperature $T_c = 10^3$ K, taking the cloud starting position at $r_0 = R$, and $\alpha = 1$ (left) and $\alpha = 0.1$ (right) as examples. The solid lines show the critical values of β for $t_{\text{cc}} = t_{\text{acc}}$ in the case of $P_{\text{ram}} > P_c$, or $t_{\text{expan}} = t_{\text{acc}}$ in the case of $P_{\text{ram}} < P_c$. Over the regime plotted $P_{\text{ram}} > P_c$, so only $t_{\text{cc}} = t_{\text{acc}}$ is shown. The dark gray regions are radiative, excluded by equation (8). Since the solid lines are always above the radiative cooling lines, for any hot flow with parameters in the non-radiative regime, the cool cloud will establish pressure equilibrium with the hot gas before being accelerated at $r_0 = R$ with $T_c = 10^3$ K. We find that this result is also valid for $T_c = 10^2$ and 10^4 K, and with varying r_0 from R to $3R$. This means that in virtually all regimes of interest, clouds reach pressure equilibrium with the hot wind on a short timescale. We use this fact in the

² The acceleration timescale t_{acc} is also called the drag timescale t_{drag} (e.g., Faucher-Giguère et al. 2012). Strictly, cool clouds can never reach the velocity of the hot wind, since the ram pressure on clouds decreases to zero while $V_c \rightarrow V_{\text{hot}}$. The acceleration of a cloud is $a_{\text{ram}} = 3(V_{\text{hot}} - V_c)^2 \rho_{\text{hot}} / (4\rho_c R_c)$, thus the acceleration timescale is estimated by

$$t_{\text{acc}} = \int_0^{V_c^{\text{upper}}} \frac{4R_c}{3V_{\text{hot}}} \left(\frac{\rho_c}{\rho_{\text{hot}}} \right) \frac{d(V_c/V_{\text{hot}})}{(1 - V_c/V_{\text{hot}})^2}, \quad (13)$$

which diverges if we integrate V_c from 0 to V_{hot} . Analytically we estimate the cool cloud velocity V_c to change from 0 to $V_{\text{upper}} = V_{\text{hot}}/2$ at a same position r , which yields Equation (13) for the time for the cloud to reach half of V_{hot} , and we say $V_c \sim V_{\text{hot}}$ in this case.

following analytical estimates. The dashed and dotted lines in Figure 1 are discussed in Section 2.3.

2.2 Pressure Equilibrium and Cloud Destruction

After pressure equilibrium with the hot flow, we can estimate whether cool clouds can be accelerated by ram pressure of the hot wind before being destroyed by hydrodynamical instabilities or thermal conduction and evaporation. We assume that after establishing pressure equilibrium at r_0 , the cloud maintains pressure balance with the hot flow as it is accelerated. Although the pressure is strongest at the front of the cloud, and proportional to $P_{\text{hot}}(1 + M_{\text{h}}^2)$, Scannapieco & Brüggén (2015) showed that an oblique shock is formed at the extended cometary wind-cloud interface and that as a result the pressure equilibrium between the hot flow and the cool cloud is best described by $P_c \approx P_{\text{hot}}(1 + M_{\text{h}})$. In our estimates below, we apply this scaling for P_c and show how the Mach number (M_{h}) of cold-hot pressure equilibrium enters the key expressions³.

Simulations show that the shocked swept-up super-shells in the central region of molecular disks quickly cool and fragment through Kelvin-Helmholtz (KH) or Rayleigh-Taylor (RT) instabilities (Strickland & Stevens 2000; Heckman et al. 2000; Fujita et al. 2009), which have comparable timescales (Krolik et al. 1981; Schiano et al. 1995). Faucher-Giguère et al. (2012) (see also Klein et al. 1994) suggested that the timescale for clouds to be destroyed by the KH instability is $t_{\text{KH}} \approx 10 t_{\text{cc}}^{\text{th}}$, where $t_{\text{cc}}^{\text{th}}$ is the crushing time of a cloud which is initially in thermal pressure equilibrium with the hot medium ($\rho_c^{\text{th}} T_c = \rho_{\text{hot}} T_{\text{hot}}$). However, recent simulations show that the cloud destruction timescale may depend on the Mach number of the flow. In particular, Scannapieco & Brüggén (2015) showed that clouds are destroyed by the KH instability only after they are shredded by other hydrodynamical instabilities. They found that the timescale for 50% of cloud to be below 2/3 of the initial cloud density is

$$t_{50} = 4 t_{\text{cc}}^{\text{th}} \sqrt{1 + M_{\text{h}}}. \quad (17)$$

Schneider & Robertson (2017) did similar high-resolution simulations of cloud destruction for both turbulent and spherical clouds, and found a longer lifetime for spherical clouds. The difference is caused by the different treatment of cooling in the simulations. In Scannapieco & Brüggén (2015) the clouds only allow cooling above $T_c \gtrsim 10^4$ K with the assumption of complete ionization, but in Schneider & Robertson (2017) the temperature of the post-shock gas can be down to ~ 100 K. Here, we follow Scannapieco & Brüggén (2015) and assume that a cloud is destroyed on the shredding timescale

$$\begin{aligned} t_{\text{sh}} &\approx \kappa \left(\frac{\rho_c^{\text{th}}}{\rho_{\text{hot}}} \right)^{1/2} \frac{R_c^{\text{th}}}{V_{\text{hot}}} (1 + M_{\text{h}})^{1/2} \\ &\approx 3.1 \times 10^2 \text{ yr } \kappa_4 (1 + M_{\text{h}})^{-1/6} \rho_0^{-1/2} u_0^{-1} P_0^{-1/2} \\ &\quad \times \alpha^{-1/2} \beta^{-1/2} N_{\text{H},21}^c T_{c,3}^{1/2} R_{200\text{pc}}^2 \text{SFR}_1^{-1}, \end{aligned} \quad (18)$$

³ Note that if one were to employ $P_c \approx P_{\text{hot}}(1 + M_{\text{h}}^2)$ for cloud pressure equilibrium, one finds higher pressures, smaller cloud radii, and more rapid destruction by hydrodynamical instabilities (equation 18), leading to even smaller maximum cloud velocities (equations 20 and 25).

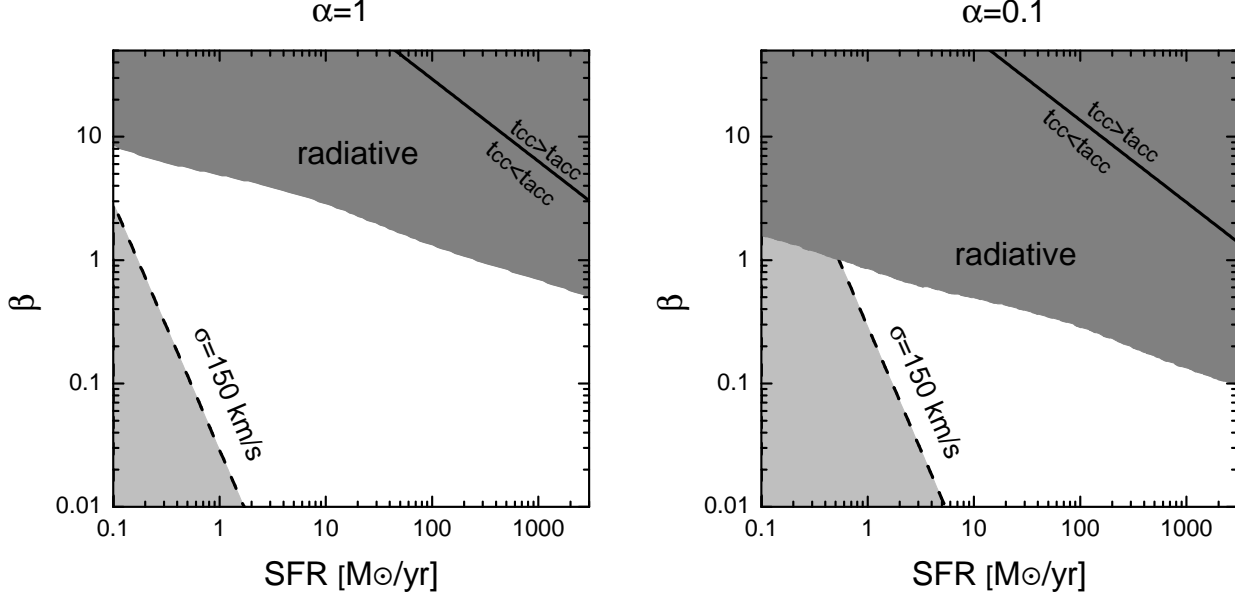


Figure 1. Timescale constraints and the gravity constraint as a function of SFR for clouds with $\alpha = 1$ (left) and $\alpha = 0.1$ (right), $T_c = 10^3$ K, and the starting position $r_0 = R$. Solid lines are the combined constraint of $t_{cc} = t_{acc}$ and $t_{expan} = t_{acc}$ (equations 15, 16). Dashed lines are the gravity constraint (equation 32). The dark gray region shows where the flow is radiative (equation 8), and the light gray region is excluded by the gravity constraint with $N_{\text{H}}^{\text{i}} = 10^{20}$ cm $^{-2}$ and $\sigma = 150$ km s $^{-1}$.

where $\kappa_4 = \kappa/4$ is a constant. After this time the cloud is considered to be destroyed. We use $T_c = 10^3 T_{c,3}$ K as the fiducial value. A turbulent cloud can be considered to have a lower temperature or a lower κ , which gives a shorter timescale of t_{sh} . Comparing the two timescales t_{sh} and t_{acc} in the case of pressure equilibrium, we find that if

$$\beta \leq 9.5 \times 10^3 (1 + M_{\text{h}})^{1/3} P_0 \rho_0^{-1} \alpha \kappa_4^{-2} T_{c,3}^{-1}, \quad (19)$$

then $t_{\text{sh}} \leq t_{\text{acc}}$, and the cloud should be shredded before acceleration to V_{hot} . Note that the factor P_0/ρ_0 strongly decreases with radius, such that $(1 + M_{\text{h}})^{1/3} P_0 \rho_0^{-1} \simeq 0.4 - 0.08$ for $r_0 = R$ to $3R$. Since $\beta \lesssim 1$ is required for hot winds from the X-ray constraints presented in Zhang et al. (2014), equation (19) is a strong constraint. It implies that t_{sh} is essentially always longer than t_{acc} for $\kappa \lesssim 390(1 + M_{\text{h}})^{1/6} P_0^{1/2} \rho_0^{-1/2} \alpha^{1/2} T_{c,3}^{-1/2}$. More discussion of larger κ and its implications for our results is given in Section 3.2. In the β -SFR plane shown in the two panels of Figure 1, equation (19) is a horizontal line off the top of both plots; for the fiducial model, t_{sh} is always much smaller than t_{acc} .

We can then estimate the maximum velocity V_c , and the “flying distance” Δr of the cloud, i.e., the distance between the cloud starting position r_0 to its destruction position $r_0 + \Delta r$, accelerated in a timescale of t_{sh} respectively. If the cloud is destroyed by the shredding timescale, we have

$$\begin{aligned} V_c^{\text{sh}} &= a_c t_{\text{sh}} = \frac{3}{4} \kappa V_{\text{hot}} \left(\frac{\rho_c}{\rho_{\text{hot}}} \right)^{-1/2} (1 + M_{\text{h}})^{1/3} \\ &\approx 10 \text{ km s}^{-1} M_{\text{h}} (1 + M_{\text{h}})^{-1/6} \kappa_4 T_{c,3}^{1/2}, \end{aligned} \quad (20)$$

$$\begin{aligned} \Delta r_{\text{sh}} &= \frac{1}{2} a_c t_{\text{sh}}^2 = \frac{3}{8} \kappa^2 R_c (1 + M_{\text{h}})^{2/3} \\ &\approx 1.1 \times 10^{-3} \text{ pc } P_0^{-1} (1 + M_{\text{h}})^{-1/3} \kappa_4^2 \\ &\quad \times \alpha^{-1/2} \beta^{-1/2} N_{\text{H},21}^c T_{c,3} R_{200\text{pc}}^2 \text{SFR}_1^{-1}, \end{aligned} \quad (21)$$

where a_c is the acceleration of the cloud. Note that V_c^{sh} is only a function of κ and T_c , and is always below 100 km s $^{-1}$ for the fiducial model. For $r_0 = R$ ($3R$) with $R = 200$ pc we have $\Delta r_{\text{sh}} \approx 0.03(2)$ pc $N_{\text{H},21}^c T_{c,3} \text{SFR}_1^{-1}$, as long as Δr is small compared with R . These results show that the cloud is destroyed very near its starting position with a low velocity V_c^{sh} , but with a strong dependence on κ . Because $M_{\text{h}} \propto r^{2/3}$ in the CC85 model, the maximum velocity $V_c^{\text{sh}} \propto M_{\text{h}}^{5/6} \propto r^{5/9}$, thus the starting position of cloud is important, especially for large starting position r_0 (see Section 3.1).

Thermal conduction may also be important to evaporate the clouds (e.g., Cowie & McKee 1977; Krolik et al. 1981; Brüggen & Scannapieco 2016). Following Brüggen & Scannapieco (2016), we adopt the timescale for cloud evaporation

$$t_{\text{evap}} \approx \frac{100}{f(M_{\text{h}})} \left(\frac{\rho_c^{\text{th}}}{\rho_{\text{hot}}} \right)^{-1/2} \frac{2g}{\sqrt{1+4g-1}}, \quad (22)$$

where the functions $f(M_{\text{h}})$ and g are given in Brüggen & Scannapieco (2016) (see their equations 11 and 19). Using the cloud and hot flow parameters we find that

$$\begin{aligned} t_{\text{evap}} &\approx 22 \text{ yr } (1 + M_{\text{h}})^{-1/3} M_{\text{h}}^{-1/2} P_0^{-3/4} u_0^{-1} \rho_0^{-1/4} \\ &\quad \times \alpha^{-3/4} \beta^{-1/4} (N_{\text{H},21}^c)^{1/2} T_{c,3}^{3/4} R_{200\text{pc}}^2 \text{SFR}_1^{-1}. \end{aligned} \quad (23)$$

Setting $t_{\text{evap}} \leq t_{\text{acc}}$ implies an upper limit on β of

$$\beta \leq 1.5 \times 10^4 (1 + M_{\text{h}})^{4/9} M_{\text{h}}^{2/3} P_0 \rho_0^{-1} \alpha (N_{\text{H},21}^c)^{2/3} T_{c,3}^{-1}. \quad (24)$$

The dimensionless factor $(1 + M_{\text{h}})^{4/9} M_{\text{h}}^{2/3} P_0 \rho_0^{-1} \sim 0.41 - 0.28$ from $r_0 = R$ to $3R$ (see Table 2). The constraint on β given by equation (24) is always stronger than the constraint given in equation (19) for the cloud shredding timescale unless $N_{\text{H}}^c \leq 5 \times 10^{20}$ cm $^{-2}$ $(1 + M_{\text{h}})^{-1/6} M_{\text{h}}^{-1} \kappa_4^{-2}$. In Section 2.3 we combine a constraint on N_{H}^c derived by comparing the

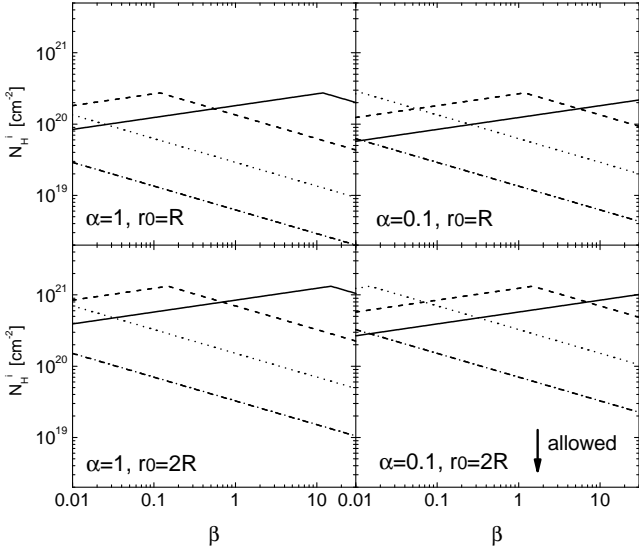


Figure 2. Constraint on initial cloud column density N_{H}^{i} as a function of β for $\alpha = 1$ (left panels) and $\alpha = 0.1$ (right panels) and for $r_0 = R$ (upper panels) and $r_0 = 2R$ (lower panels), for $R = 200$ pc, SFR = $1 M_{\odot} \text{ yr}^{-1}$ (solid), $10 M_{\odot} \text{ yr}^{-1}$ (dashed), $100 M_{\odot} \text{ yr}^{-1}$ (dotted), $1000 M_{\odot} \text{ yr}^{-1}$ (dash-dotted) and taking $N_{\text{H}}^{\text{obs}} = 10^{21} \text{ cm}^{-2}$ (see equations 33 and 34), $\sigma = 150 \text{ km s}^{-1}$.

gravitational and ram pressure forces on clouds, and show that equation (24) always holds for cool clouds accelerated outwards by adiabatic hot winds.

The evaporation may play an important role in destroying the cloud. The maximum velocity of the cloud if it is subject to only evaporation is

$$\begin{aligned} V_c^{\text{evap}} &= a_c t_{\text{evap}} = \frac{3V_{\text{hot}}^2}{4R_c} \left(\frac{\rho_{\text{hot}}}{\rho_c} \right) t_{\text{evap}} \\ &\approx 0.6 \text{ km s}^{-1} M_{\text{h}}^{-1/2} (1 + M_{\text{h}})^{-1/3} P_0^{-3/4} u_0 \rho_0^{3/4} \\ &\quad \times \alpha^{-1/4} \beta^{1/4} (N_{\text{H},21}^{\text{i}})^{-1/2} T_{c,3}^{3/4}, \end{aligned} \quad (25)$$

which is significant lower than V_c^{sh} given by equation (20). The distance traveled before destruction is

$$\begin{aligned} \Delta r_{\text{evap}} &= \frac{1}{2} a_c t_{\text{evap}}^2 \\ &\approx 7 \times 10^{-5} \text{ pc } M_{\text{h}}^{-1} (1 + M_{\text{h}})^{-2/3} P_0^{-3/2} \rho_0^{1/2} \\ &\quad \times \alpha^{-1} T_{c,3}^{3/2} R_{200\text{pc}}^2 \text{SFR}_1^{-1}, \end{aligned} \quad (26)$$

These conclusions of low V_c and small δr are essentially similar as for the cloud destroyed by shredding. If thermal condition is important, the cloud is even more difficult to be accelerated than the non-conduction case.

2.3 Constraints on Cloud Column Density from Gravity

In the case of $V_{\text{hot}} \gg V_c$, where V_c is the velocity of the cool cloud, the ram pressure force at the front of the cloud is $F_{\text{ram}} \approx \rho_{\text{hot}} V_{\text{hot}}^2 A_c$, where $A_c = \pi R_c^2$ is the projected area of the cloud. In order for the cloud to be accelerated by the hot

flow, the ram pressure must be stronger than gravity after pressure equilibrium is established. For simplicity if we take an isothermal sphere model for the gravitational potential of the galaxy with $M_{\text{gal}}(r) = 2\sigma^2 r/G$, where σ is the velocity dispersion of the galaxy, the gravitational force is

$$F_{\text{grav}} = 2\sigma^2 M_c / r, \quad (27)$$

where $M_c = 4\pi\rho_c R_c^3/3$ is the total mass of the cloud. The requirement $F_{\text{ram}} > F_{\text{grav}}$ gives a constraint on the column density of the cloud after pressure equilibrium of

$$N_{\text{H},21}^c \leq 8.2 (u_0 r_{0,*}^{-1}) \alpha^{1/2} \beta^{1/2} \sigma_{150}^{-2} R_{200\text{pc}}^{-1} \text{SFR}_1, \quad (28)$$

where $r_{0,*} = r_0/R$ is the dimensionless radial starting position of the cloud (see Table 2). Combining equation (28) with (24) to eliminate the column density dependence, we find that the constraint on β for $t_{\text{evap}} \leq t_{\text{acc}}$ is

$$\begin{aligned} \beta &\leq 1.5 \times 10^7 \left(\frac{u_0}{r_{0,*}} \right) (1 + M_{\text{h}})^{2/3} M_{\text{h}} P_0^{3/2} \rho_0^{-3/2} \\ &\quad \times \alpha^2 \sigma_{150}^{-2} T_{c,3}^{-3/2} R_{200\text{pc}}^{-1} \text{SFR}_1. \end{aligned} \quad (29)$$

We find that the constraint of β given by equation (29) is always in the radiative region of the (SFR, β) parameter space, which means that the cloud will always be destroyed before being accelerated for non-radiative hot winds.

For simplicity, if we assume the initial cloud is compressed by the ram pressure of the hot wind in a timescale of t_{cc} (equation 11) and comes into pressure equilibrium with the hot wind, we can relate the hydrogen density and column density of the cloud after pressure equilibrium (n_{H}^c and N_{H}^c) to its initial values (n_{H}^{i} and N_{H}^{i}):

$$n_{\text{H}}^c = 8.5 \times 10^5 \text{ cm}^{-3} (1 + M_{\text{h}}) P_0 \alpha^{1/2} \beta^{1/2} R_{200\text{pc}}^{-2} T_{c,3}^{-1} \text{SFR}_1, \quad (30)$$

and

$$\begin{aligned} N_{\text{H}}^c &= 90 N_{\text{H}}^{\text{i}} \xi^{2/3} (1 + M_{\text{h}})^{2/3} P_0^{2/3} \alpha^{1/3} \beta^{1/3} R_{200\text{pc}}^{-4/3} \\ &\quad \times (n_{\text{H},3}^{\text{i}})^{-2/3} T_{c,3}^{-2/3} \text{SFR}_1^{2/3} \end{aligned} \quad (31)$$

respectively. Simulations shows that the compression of the cloud is almost completely perpendicular to the hot flow, thus we introduce a factor $\xi = R_c^{\parallel}/R_c^{\perp}$ in equation (31), where R_c^{\parallel} and R_c^{\perp} are the radius of the cloud parallel and perpendicular to the flow respectively. Typically in the simulations of Scannapieco & Brügggen (2015), $R_c^{\parallel}/R_c^{\perp} \sim 8$ on a timescale of t_{sh} .

Using Equations (30) and (31), the Eddington-like limit given by the constraint $F_{\text{ram}} \geq F_{\text{grav}}$ then translates into a constraint on β :

$$\begin{aligned} \beta &\geq 113 (1 + M_{\text{h}})^4 M_{\text{h}}^{-8} \rho_0 u_0^{-1} \alpha^{-1} \xi^4 (N_{\text{H},21}^{\text{i}})^6 (n_{\text{H},3}^{\text{i}})^{-4} \\ &\quad \times T_{c,4}^{-3} \sigma_{150}^{12} R_{200\text{pc}}^{-2} \text{SFR}_1^{-2}. \end{aligned} \quad (32)$$

For simplicity we take $\xi = 1$, which gives a lower limit on the *minimum* value of β required for acceleration. The dotted lines in Figure 1 show this limit at $r_0 = R$ for $\sigma = 150 \text{ km s}^{-1}$ and clouds with initial $N_{\text{H}}^{\text{i}} = 10^{20} \text{ cm}^{-2}$, where the light gray regions are excluded by equation (32). Since the Eddington-like limit on β is extremely sensitive to virtually all of the parameters of the problem ($\beta \propto (N_{\text{H}}^{\text{i}})^6$ in equation 32), clouds with initial $N_{\text{H}}^{\text{i}} = 10^{21} \text{ cm}^{-2}$ are unlikely to be accelerated at $r_0 = R$ because of gravity. However, note that since the critical value of β is so sensitive to the set of parameters, the gravity constraint at fixed σ is weak.

The strong ξ and N_{H} dependence of β in equation (32) implies that simulations of cloud acceleration and destruction should be explored including the effects of gravity.

If we take α , β and σ as fixed parameters, equation (32) can be written as a constraint on the initial cloud column density N_{H}^{i} such that $F_{\text{ram}} \geq F_{\text{grav}}$:

$$N_{\text{H},21}^{\text{i}} \leq 0.41(1 + M_{\text{h}})^{-2/3} M_{\text{h}} u_0^{1/2} P_0^{-1/6} \alpha^{1/6} \beta^{1/6} \times (n_{\text{H},3}^{\text{i}})^{2/3} T_{\text{c},3}^{2/3} \sigma_{150}^{-2} R_{200\text{pc}}^{1/3} \text{SFR}_1^{1/3}, \quad (33)$$

which gives an upper bound on the initial cloud column density N_{H}^{i} for ejection from a galaxy, where the dimensionless factor $(1 + M_{\text{h}})^{-2/3} M_{\text{h}} u_0^{1/2} P_0^{-1/6}$ increases from ~ 0.9 to 6.6 from $r_0 = R$ to $r_0 = 3R$ (Table 2).

On the other hand, N_{H}^{i} can be constrained by observations. The measured Na D or Mg II column density in the outflows of LIRGs and ULIRGs gives a constraint on the observationally-derived total hydrogen column density of $N_{\text{H}}^{\text{obs}} \sim 10^{20} - 10^{21} \text{ cm}^{-2}$, with an order of magnitude uncertainty due to the metallicity of the gas, the Na depletion factor, and the Na ionization correction (e.g., Heckman et al. 2000; Schwartz & Martin 2004; Rupke et al. 2002; Rupke et al. 2005b; Martin 2005; Martin 2006; Murray et al. 2007). It has been shown that the atomic absorption lines are optically thick, with a typical covering factor of $C_f \sim 0.2 - 1$. Assuming the apparent column density of the cloud obtained by observation is $N_{\text{H}}^{\text{obs}}$, with an amplification factor of C_f^{-1} , the total column density along the line of sight $N_{\text{H}}^{\text{obs}} C_f^{-1}$ is contributed to by multiple overlapping single clouds with a column density of N_{H}^{c} , thus we have $N_{\text{H}}^{\text{c}} \leq N_{\text{H}}^{\text{obs}} C_f^{-1}$, which gives

$$N_{\text{H},21}^{\text{i}} \leq 0.01(1 + M_{\text{h}})^{-2/3} P_0^{-2/3} \alpha^{-1/3} \beta^{-1/3} N_{\text{H},21}^{\text{obs}} C_f^{-1} \times (n_{\text{H},3}^{\text{i}})^{2/3} R_{200\text{pc}}^{4/3} T_{\text{c},3}^{2/3} \text{SFR}_1^{-2/3}. \quad (34)$$

Figure 2 demonstrates examples on the upper bounds on N_{H}^{i} as a function of β for various SFR and α , where we choose a typical value for $N_{\text{H}}^{\text{obs}} = 10^{21} \text{ cm}^{-2}$, a covering factor of $C_f = 0.5$, and $T_{\text{c}} = 10^3 \text{ K}$, $n_{\text{H}}^{\text{i}} = 10^3 \text{ cm}^{-3}$, $R = 200 \text{ pc}$ and $\sigma = 150 \text{ km s}^{-1}$ in equations (33) and (34). Higher SFR yields a more stringent constraint on β and N_{H}^{i} . The constraint on N_{H}^{i} is weaker for larger initial cloud launch radius r_0 . For example, N_{H}^{i} is always $N_{\text{H}}^{\text{i}} \lesssim 3 \times 10^{20} \text{ cm}^{-2}$ at $r_0 = R$. For $\text{SFR} \gtrsim 100 M_{\odot} \text{ yr}^{-1}$, $N_{\text{H}}^{\text{i}} \lesssim 2 \times 10^{20} \text{ cm}^{-2}$ at $r_0 = R$ and $N_{\text{H}}^{\text{i}} \lesssim 10^{21} \text{ cm}^{-2}$ at $r_0 = 2R$. Note that the constraint of $N_{\text{H}}^{\text{i}} \lesssim 10^{20} - 10^{21} \text{ cm}^{-2}$ is given for the fiducial parameter set. Higher values of T_{c} , n_{H}^{i} , or R can increase the upper bound on N_{H}^{i} . For example, for $T_{\text{c}} = 10^4 \text{ K}$ and $R = 1 \text{ kpc}$, we derive that $N_{\text{H}}^{\text{i}} \lesssim 10^{22} \text{ cm}^{-2}$.

However, note that because both $N_{\text{H}}^{\text{obs}}$ and C_f have an order of magnitude uncertainty, the constraint given by Equation (34) has at least one order of magnitude uncertainty. Even so, we find that, in general N_{H}^{i} is constrained to be $N_{\text{H}}^{\text{i}} \lesssim 10^{20} - 10^{22} \text{ cm}^{-2}$ ($n_{\text{H}}^{\text{i}})^{2/3} T_{\text{c}}^{2/3}$ for $R \geq 200 \text{ pc}$ over a broad range of SFR.

3 NUMERICAL SOLUTIONS OF THE RAM PRESSURE ACCELERATION OF COOL CLOUDS

3.1 Fiducial Model

In this section we calculate the cloud evolution numerically. Assuming that ram pressure dominates the driving of cool gas clouds, the equation of motion for a cloud of cool gas is

$$M_{\text{c}} \frac{dV_{\text{c}}}{dt} = \dot{M}_{\text{hot}} V_{\text{hot}} \left(1 - \frac{V_{\text{c}}}{V_{\text{hot}}} \right)^2 \frac{A_{\text{c}}}{\Omega r^2} - \frac{GM_{\text{gal}}(r)M_{\text{c}}}{r^2}, \quad (35)$$

where \dot{M}_{hot} is the mass-loss rate of the hot wind, Ω is the solid angle subtended by hot wind fluid, and $M_{\text{gal}}(r)$ is the mass of the galaxy. For the spherical model $\Omega = 4\pi$. The cloud radius R_{c} evolves as a function of time in response to the cloud's internal pressure P_{c} and the surrounding hot fluid. For $P_{\text{hot}}(1 + M_{\text{h}}) < P_{\text{c}}$ we use

$$\frac{dR_{\text{c}}}{dt} = \sqrt{\frac{k_{\text{B}} T_{\text{c}}}{m_{\text{H}}}} \left[1 - \frac{P_{\text{hot}}(1 + M_{\text{h}})}{P_{\text{c}}} \right]^{1/2} \quad (36)$$

On the other hand, if $P_{\text{hot}}(1 + M_{\text{h}}) > P_{\text{c}}$, the cloud is compressed. As mentioned in Section 2.3, in this case the compression of the cloud is almost completely perpendicular to the hot flow, we use

$$\frac{dR_{\text{c}}^{\perp}}{dt} = -\sqrt{\frac{k_{\text{B}} T_{\text{c}}}{m_{\text{H}}}} \left[\frac{P_{\text{hot}}(1 + M_{\text{h}})}{P_{\text{c}}} - 1 \right]^{1/2} \quad (37)$$

for $P_{\text{hot}}(1 + M_{\text{h}}) > P_{\text{c}}$, where R_{c}^{\perp} is the radius of the cloud perpendicular to the flow. As in Sections 2.2 and 2.3, we take the pressure on the cloud to be $P_{\text{hot}}(1 + M_{\text{h}})$ when calculating pressure equilibrium with the hot gas, even though the ram pressure at the head of the cloud is proportional to $\rho_{\text{hot}} V_{\text{hot}}^2$, consistent with the numerical results of Scannapieco & Brügggen (2015). For a given parameter set of (α, β) , r_0 , and SFR, the cloud velocity V_{c} can be calculated by solving equations (35), (36) and (37). We require $t_{\text{sh}} > t$ in the calculation, otherwise the cloud should be destroyed and the calculation stops. If t_{evap} is taken into account and $t_{\text{evap}} < t_{\text{sh}}$, we have an even more stringent constraint on the maximum velocities V_{c} .

We start by calculating the cloud evolution for the fiducial model ($\kappa = 4$) for cloud destruction based on high-resolution hydrodynamical simulations (equation 18), and compare with the analytical results in Section 2. Figure 3 gives examples of solutions for V_{c} , the ratio $V_{\text{c}}/V_{\text{hot}}$ as functions of time, and V_{c} as a function of radius for different cloud properties: $T_{\text{c}} = 10^3 \text{ K}$ (upper panels), $T_{\text{c}} = 10^4 \text{ K}$ (lower panels). We choose $(\alpha, \beta) = (1, 1)$, a host galaxy with $R = 200 \text{ pc}$, $\text{SFR} = 10 M_{\odot} \text{ yr}^{-1}$, $\sigma = 150 \text{ km s}^{-1}$, cloud column density after pressure equilibrium of $N_{\text{H}}^{\text{c}} = 10^{20} \text{ cm}^{-2}$ (blue lines) and 10^{21} cm^{-2} (black lines), and the start position of the cloud to be $r_0 = R, 2R,$ and $3R$ (solid, dashed, and dotted, respectively). The calculation stops when $t = t_{\text{sh}}$. Figure 3 shows that the cloud maximum velocities V_{c} mainly depend on T_{c} and r_0 . Different N_{H}^{c} changes the cloud trajectories but not the maximum V_{c} . Clouds with $T_{\text{c}} = 10^3 \text{ K}$ can only be accelerated to $\Delta r/R \sim 10^{-3}$ (0.2 pc) and $\sim 10^{-2}$ (2 pc) for $N_{\text{H}}^{\text{c}} = 10^{20} \text{ cm}^{-2}$ and 10^{21} cm^{-2} , respectively. Clouds with $T_{\text{c}} \approx 10^4 \text{ K}$ can be accelerated to $\Delta r \sim 0.1 R$ (20 pc) for $N_{\text{H}}^{\text{c}} = 10^{21} \text{ cm}^{-2}$ and $r_0 = 3R$, a bit larger than the values of Δr for $T_{\text{c}} = 10^3 \text{ K}$. These results

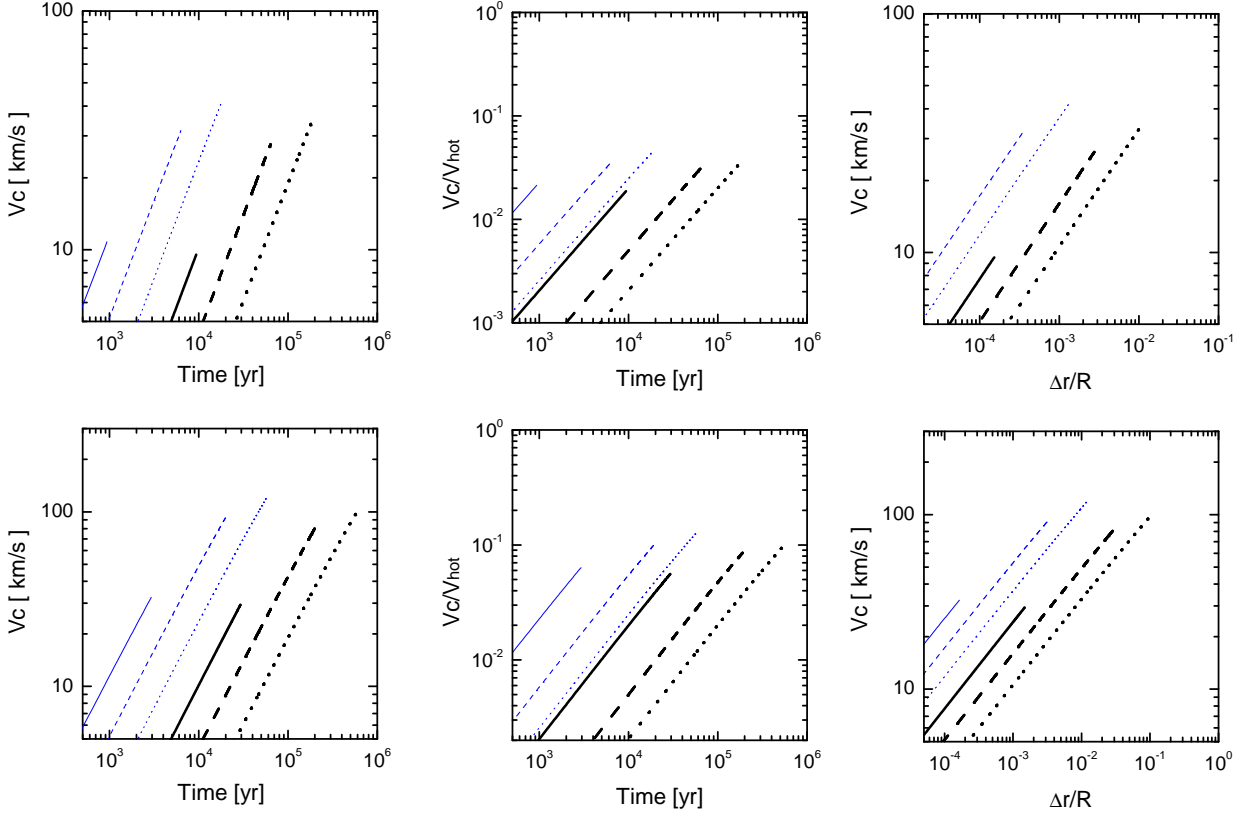


Figure 3. Velocity of a cool cloud V_c and V_c/V_{hot} as functions of time (left two panels), and V_c as a function of radius $\Delta r/R$ (right panels) with cloud temperature $T_c = 10^3$ K (upper panels), $T_c = 10^4$ K (lower panels), and $N_{\text{H}}^c = 10^{21}$ cm^{-2} (black thick lines), $N_{\text{H}}^c = 10^{20}$ cm^{-2} (blue thin lines), and starting position at $r_0 = R$ (solid lines), $2R$ (dashed lines), $3R$ (dotted lines), where $(\alpha, \beta) = (1, 1)$, and the host galaxy has $R = 200$ pc, $\text{SFR} = 10 M_{\odot} \text{yr}^{-1}$, and $\sigma = 150$ km s^{-1} .

are consistent with the analytic constraint given in equation (21). Because of a longer survival distance, the cloud with higher T_c can be accelerated to higher V_c . The maximum V_c for clouds with $T_c = 10^3$ K is limited to $V_c \sim 40$ km s^{-1} or $V_c \sim 0.04 V_{\text{hot}}$, but V_c reaches ~ 100 km s^{-1} or $V_c \sim 0.1 V_{\text{hot}}$ for clouds with $T_c = 10^4$ K, all of which are consistent with equations (20) and (21).

Figure 4 gives the more general result. It shows contours of maximum cloud velocity V_c in the parameter space of $(\log \alpha, \log \beta)$. We start the calculation for clouds with $N_{\text{H}}^c = 10^{21}$ cm^{-2} at $r_0 = R$ (left panels) and $3R$ (right panels), with $T_c = 10^3$ K (upper panels) and 10^4 K (lower panels), and $\text{SFR} = 10 M_{\odot} \text{yr}^{-1}$ with $\sigma = 150$ km s^{-1} . The calculations stop when $t = t_{\text{sh}}$ even $t_{\text{sh}} > t_{\text{evap}}$. The grey regions show the parameter regime where the flow becomes radiative and the CC85 model is not valid (see Zhang et al. 2014). We find that clouds can hardly be accelerated. The maximum value of V_c reaches ~ 200 km s^{-1} only for $T_c = 10^4$ K and $r_0 = 3R$. Otherwise V_c is always below 100 km s^{-1} . Note that V_c slightly depends on (α, β) , which is different from the analytic estimate in equation (20). This is because of gravity: for fixed T_c and r_0 , higher thermalization efficiency α general gives higher V_c . The critical lines of $V_c = 0$ are given by equation (28). Overall, the entire lower left region of each panel produces no positive acceleration for

the clouds because the ram pressure force does not exceed the gravitational force.

Note that because V_c is an increasing function of M_{h} (equation 20), clouds with larger starting position can be accelerated to higher V_c . For example, for clouds with $r_0 = 10R$ with $R = 200$ pc and $N_{\text{H}}^c = 10^{20}$ cm^{-2} , we find that V_c reaches $\sim 200 - 300$ km s^{-1} . This result is consistent with numerical simulations (Scannapieco & Brüggen 2015). Although very large values of r_0 might be reasonable for nearby halo gas or clouds over run by the hot wind after escaping the galaxy, in this paper we focus on clouds accelerated out of the host galaxy ($r_0 \leq 3R$).

3.2 Magnetic Fields and Large κ

In Sections 2 and 3.1 we assume the pressure equilibrium condition is $P_c = P_{\text{hot}}(1 + M_{\text{hot}})$ (equations 30 and 31), and show that the most important timescales determining the terminal velocity of cool clouds is the cloud shredding timescale (equations 18, 19 and 20). Magnetic fields may change the structure of clouds, and potentially suppress the cloud shredding instability. We compare the thermal pressure P_c with the magnetic pressure inside the cloud, and find that if

$$B \geq B_{\text{crit}} = 1.7 \text{ mG } P_0^{1/2} (1 + M_{\text{h}})^{1/2} \alpha^{1/4} \beta^{1/4} R_{200\text{pc}}^{-1} \text{SFR}_1^{1/2}, \quad (38)$$

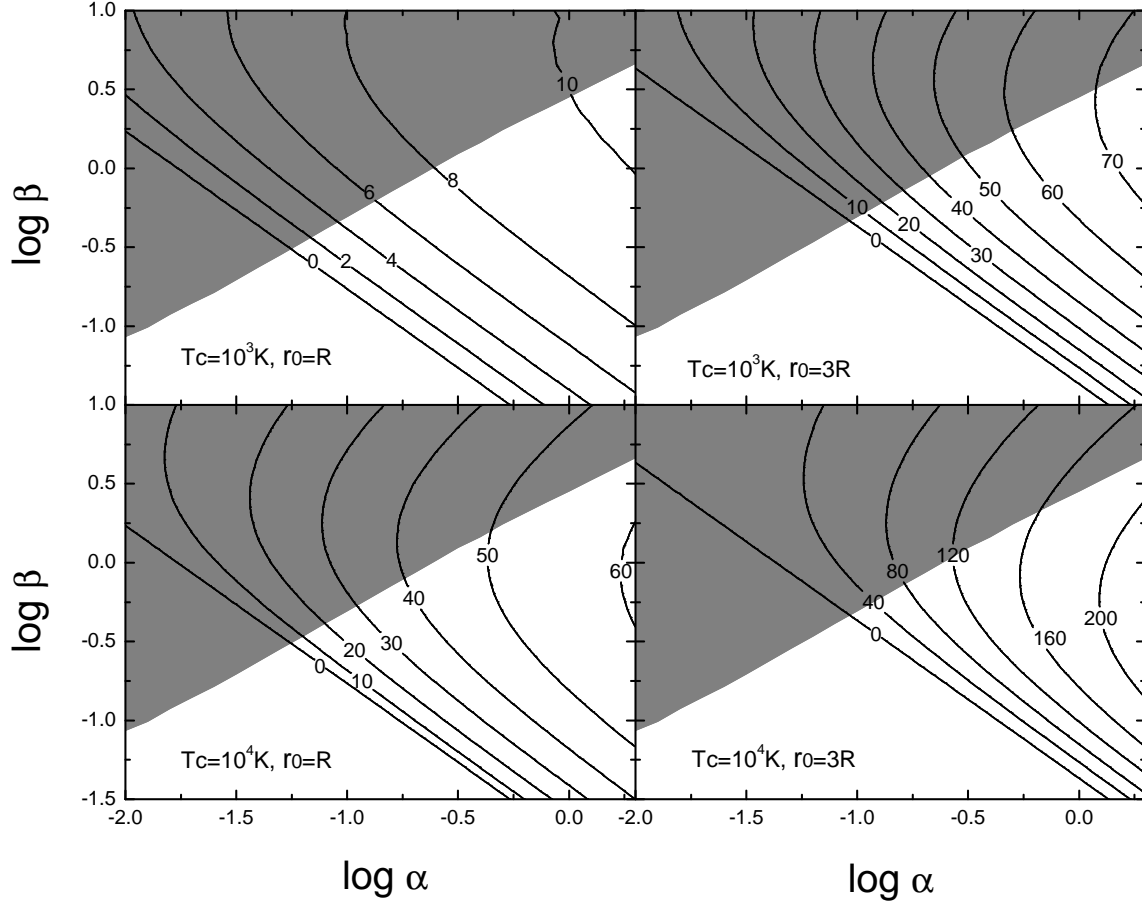


Figure 4. Contours of the maximum velocity of cool gas V_c (km s^{-1}) in the parameter space of $(\log \alpha, \log \beta)$, with cloud starting position $r_0 = R$ (left panels), $3R$ (right panels) with $R = 200$ pc, $T_c = 10^3$ (upper panels) and $T_c = 10^4$ K (lower panels), where $N_H^c = 10^{21} \text{ cm}^{-2}$, and host galaxy $\text{SFR} = 10 M_\odot \text{ yr}^{-1}$ and $\sigma = 150 \text{ km s}^{-1}$. The shaded regions indicate that the solution is radiative at R . The contours go to $V_c = 0$ in the lower left region of each panel because of the gravity constraint of equation (28).

the magnetic pressure dominates over the thermal pressure inside the cloud. Although this value of the internal cloud field is very large compare to normal star-forming galaxies and starbursts (Thompson et al. 2006), a strong field may be generated in the rapidly cooling shock with the hot wind that initially establishes pressure equilibrium.

Magnetic fields may also suppress the cloud shredding and the KH instability, and yield a larger value of κ . Recent magnetohydrodynamic simulations show that κ may be larger than the value of 4 implied by high-resolution hydrodynamical simulations because of cloud magnetization (e.g., McCourt et al. 2015)⁴. For this reason, although we

take $\kappa = 4$ in our fiducial models, the effects of larger κ and its implications for our results should be discussed.

Equation (19) implies that the critical value of κ such that $t_{\text{sh}} \sim t_{\text{acc}}$ is

$$\kappa_{\text{crit}} \sim 390(1 + M_h)^{1/6} P_0^{1/2} \rho_0^{-1/2} \alpha^{1/2} T_{c,3}^{-1/2}, \quad (39)$$

where the dimensionless factor $(1 + M_h)^{1/6} P_0^{1/2} \rho_0^{-1/2} \alpha^{1/2} \sim 0.61 - 0.29$ for $r_0 = R$ to $3R$. This gives an analytic estimate of the required κ for significant cloud acceleration. However, as discussed in Section 2.2 (equations 25 and 26), saturated evaporation may play an important role in cloud destruction if cloud shredding is suppressed. The estimates in Section 2.2 imply that saturated conduction limits $V_c \lesssim 100 \text{ km s}^{-1}$. In fact, the presence of magnetic fields may simultaneously suppress both conduction and the cloud shredding (e.g., Orlando et al. 2008). For these reasons, and because of the evaporation timescale is similar to the cloud shredding timescale, in the following we neglect cloud evaporation in

⁴ McCourt et al. (2015) show that a magnetic field in a hot wind may also enhance the ram pressure force by a factor of $\sim (1 + V_A^2/V_{\text{hot}}^2)$, where V_A is the Alfvén speed in the wind. Setting $V_A^2 \geq V_{\text{hot}}^2$ requires $B \geq 1.2 \text{ mG } u_0 \rho_0^{1/2} \alpha^{1/4} \beta^{3/4} R_{200, \text{pc}}^{-1/2} \text{SFR}_1^{1/2}$. Taking $\rho_0 \sim 10^{-2}$ at $r_0 = 2R$, $u_0 \sim 1$, $\alpha \sim \beta \sim 1$, this implies $B \gtrsim 100 \mu\text{G}$.

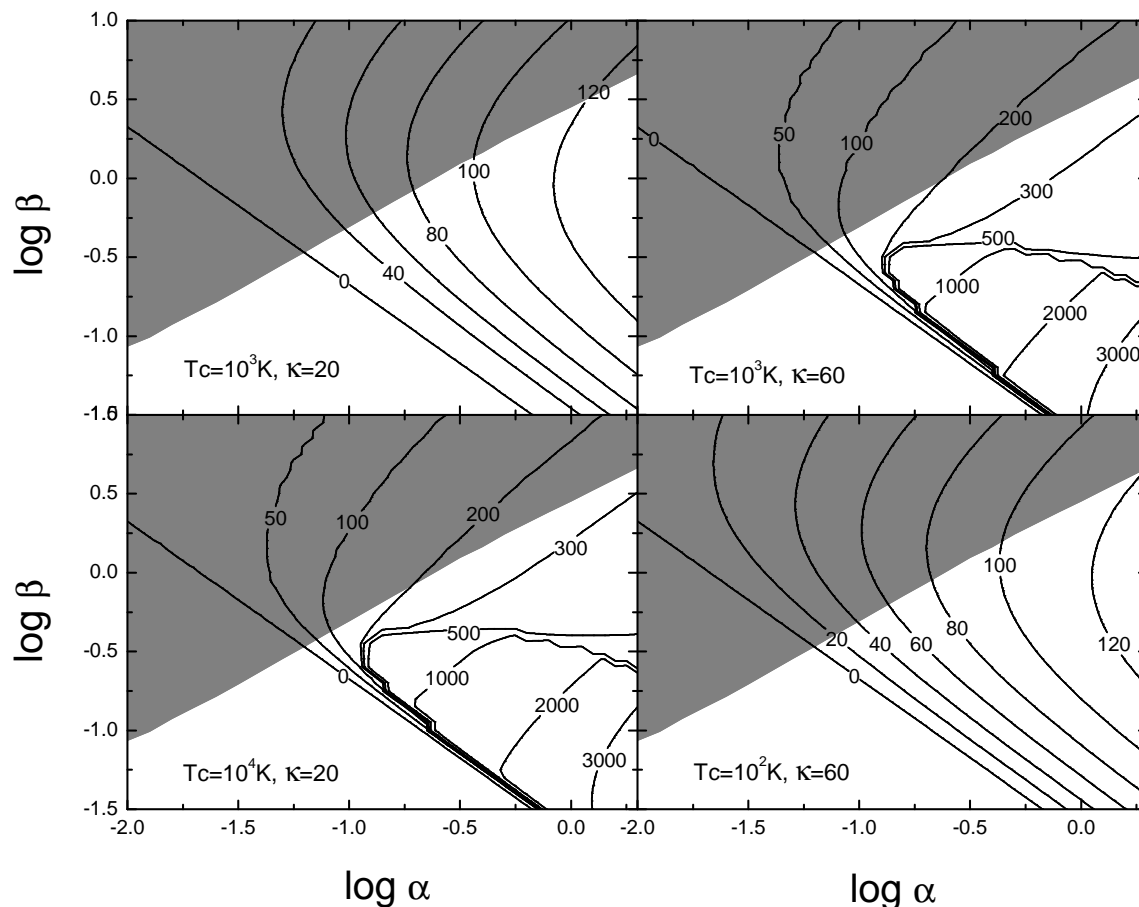


Figure 5. Contours of the maximum velocity of cool gas V_c (km s^{-1}) in the parameter space of $(\log \alpha, \log \beta)$ with various T_c and κ : $\kappa = 20$ (left panels), $\kappa = 60$ (lower panels), $T_c = 10^3$ K (upper panels), $T_c = 10^4$ K (lower left), $T_c = 10^2$ K (lower right), with cloud starting position $r_0 = 2R$, $R = 200$ pc, $\text{SFR} = 10 M_\odot \text{ yr}^{-1}$, $\sigma = 150 \text{ km s}^{-1}$, and $N_{\text{H}}^c = 10^{21} \text{ cm}^{-2}$.

our numerical experiments, and simply focus on the cloud shredding timescale.

Figure 5 shows contours of V_c in the parameter space of $(\log \alpha, \log \beta)$ with larger $\kappa = 20, 60$ and $T_c = 10^2, 10^3$ and 10^4 K. For $\kappa = 20$, a cloud with $T_c = 10^3$ K and a hot wind with $\alpha \sim 1, \beta \gtrsim 0.2$ can be accelerated to $V_c \gtrsim 100 \text{ km s}^{-1}$ (upper left), and clouds with $T_c = 10^4$ K can be accelerated to $V_c \sim 2000 \text{ km s}^{-1}$ or even higher velocities with $\alpha \sim 1, \beta \sim 0.2$. A larger value of $\kappa = 60$ can accelerate clouds with $T_c = 10^3$ K to the similar value of V_c as clouds with $T_c = 10^4$ K and $\kappa = 20$. Also, clouds with $T_c = 10^2$ K can be accelerated to $\gtrsim 100 \text{ km s}^{-1}$ for $\kappa = 60$ (lower right). Note that $\Delta r_{\text{sh}} \propto \kappa^2$ in equation (21), and thus for $r_0 = R$ ($3R$) with $R = 200$ pc, we have $\Delta r \approx 0.65(50)$ pc $N_{\text{H},21}^c T_{c,3} \text{SFR}_1^{-1}$ for $\kappa = 20$, and $\Delta r \approx 5.8$ pc (450 pc) $N_{\text{H},21}^c T_{c,3} \text{SFR}_1^{-1}$ for $\kappa = 60$. In Section 4 we compare these results with the observed cool cloud velocities.

McCourt et al. (2015) showed that for magnetized clouds κ is sufficiently large that cool clouds may become

co-moving with the hot wind, and Δr thus approaches infinity. In Section 4 we also return to this issue.

4 CASE STUDIES

Here we compare the model of RPA of cool clouds by hot winds with some observations of individual starbursts, including M82, dwarf starbursts, LIRGs and ULIRGs.

4.1 M82

M82 is perhaps the most well-studied starburst galaxy in the local Universe. The total 8-1000 μm infrared luminosity of M82 $L_{\text{IR}} \simeq 5.6 \times 10^{10} L_\odot$ (Sanders et al. 2003) corresponds to a SFR of $\sim 5 - 10 M_\odot \text{ yr}^{-1}$ (O’Connell & Mangano 1978; Kennicutt 1998; Förster Schreiber et al. 2003; Strickland et al. 2004a; Elbaz et al. 2007; Strickland & Heckman 2009; Panuzzo et al. 2010), depending on the assumed IMF. The projected velocities of the cool or warm outflow are from 40–

200 km s⁻¹ in molecular emission (H₂, Veilleux et al. 2009; SiO, García-Burillo et al. 2001; CO, Walter et al. 2002), and ~ 100 km s⁻¹ in the Na D absorption lines (Schwartz & Martin 2004), to a higher value of ~ 600 km s⁻¹ for warm H α clumps (Lehnert & Heckman 1996; Shoppell & Bland-Hawthorn 1998). Strickland & Heckman (2009) modeled the physical properties of the SN-driven hot wind based on the best currently available observations of M82. They found that the hard X-ray observations constrain the hot wind to have $\dot{M}_{\text{hot}} \sim 1.4 - 3.6 M_{\odot} \text{ yr}^{-1}$ ($\beta \sim 0.1 - 0.6$), efficient thermalization ($\alpha \sim 1$), and an implied asymptotic hot wind velocity of $V_{\text{hot}} \sim 1500 - 2000$ km s⁻¹.

As expected from our analytic estimates, we find that our fiducial model ($\kappa = 4$) is unable to explain the observed cool cloud velocities. In our calculations we take the total SFR of M82 as $10 M_{\odot} \text{ yr}^{-1}$, and adopt clouds of temperature $T_c = 10^4$ K for H α emission, $T_c = 10^3$ K for Na D absorbers, and $T_c = 100$ K for molecular emitters (see Figures 3, 4). For our fiducial parameters, the maximum cloud velocities are always below ~ 100 km s⁻¹ for $T_c = 10^3$ K, and below ~ 200 km s⁻¹ for $T_c = 10^4$ K.

Increasing the lifetime of clouds — e.g., by making κ arbitrarily large in equations (18) and (19) as discussed in Section 3.2 might solve this problem. For $\alpha = 1$, $\beta = 0.5$, $r_0 = 2R$ and $\kappa \sim 23$, we find that clouds with $T_c = 10^3$ K are accelerated to ~ 140 km s⁻¹, and clouds with $T_c = 10^4$ K reach ~ 600 km s⁻¹. However, the flying distances of clouds are $\Delta r = 30$ pc and 1.1 kpc for $T_c = 10^3$ K and $T_c = 10^4$ K, which are inconsistent with large multi-kpc extend of the emission and absorption from observations. On the other hand, if κ is large enough that the clouds become co-moving with the hot flow, as in the magnetized cloud simulations of McCourt et al. (2015), Δr becomes large enough to match observations. However, in this case, $V_c = V_{\text{hot}} \sim 1500 - 2000$ km s⁻¹ and the cool cloud velocities are then too high to match observations (e.g., Leroy et al. 2015). We conclude that the acceleration profile, radial extent, and asymptotic velocity of cool clouds may be used as a strong constraint on any models of ram pressure acceleration.

4.2 Dwarf Starbursts

The typical outflow velocities of dwarf starburst galaxies are in the range of $V_c \sim 20 - 200$ km s⁻¹ (Marlowe et al. 1995; Martin 1998; Schwartz & Martin 2004; Keeney et al. 2006). In particular, the Na D absorbers in the sample of Schwartz & Martin (2004) (NGC 1569, NGC 4214, NGC 4449) have low velocities $V_c \sim 40 - 50$ km s⁻¹, which may be explained by the CC85 model combined with the RPA scenario and additional observational constraints on the diffuse X-ray emission from these systems. We search for cool cloud wind solutions in these systems over a wide range of α and β , and assuming cool cloud properties as follows: $r_0 = 2R$, $T_c = 10^3$ K, $N_{\text{H}}^c = 10^{21}$ cm⁻². We find that clouds in the three dwarf starbursts can never be accelerated to $40 - 50$ km s⁻¹ if we use the fiducial destruction timescale in equation (17). However, we still find solutions for some dwarf star-

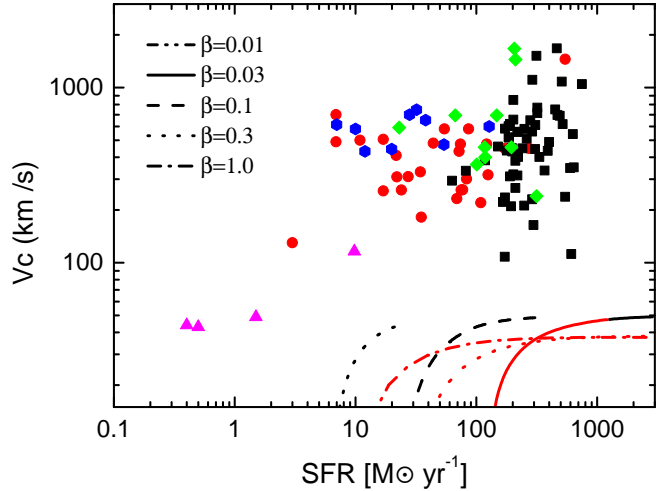


Figure 6. The relation between V_c and SFR (combined equations 35, 36 or 37, and 41) for α ranging from 10^{-2} to 2, but with fixed $\beta = 0.01, 0.03, 0.1, 0.3$ and 1, black lines are for adiabatic winds, and red lines are formally in the radiative region and the model breaks down. The parameter set is taken as $r_0 = 2R$, $R = 200$ pc, $N_{\text{H}}^c = 10^{21}$ cm⁻², $T_c = 10^3$ K, $f_d = 0.1$, $\sigma = 150$ km s⁻¹ and $\kappa = 4$. The galactic outflow data are the maximum velocities taken from dwarf starbursts (*triangles*, Schwartz & Martin 2004), LIRGs (*circles*, Heckman et al. 2000; Rupke et al. 2005b), ULIRGs (*squares*, Rupke et al. 2002, 2005b; Martin 2005), AGN ULIRGs (*diamonds*, Rupke et al. 2005c), High- z star forming (*hexagons*, Weiner et al. 2009; Erb et al. 2012; Kornei et al. 2013).

bursts if we use a slightly longer destruction timescale $\kappa = 6$ instead of 4 that $t_{\text{sh}} = 6t_{\text{cc}}^{\text{th}}\sqrt{1 + \overline{M}_{\text{h}}}$.⁵

NGC 1569 has a diffuse X-ray luminosity $\simeq 1.4 \times 10^{38}$ erg s⁻¹ (Ott et al. 2005) and we take SFR = $0.4 M_{\odot} \text{ yr}^{-1}$, $R = 100$ pc and (very low) $\sigma = 25$ km s⁻¹ (Stil & Israel 2002; Ott et al. 2005; Pasquali et al. 2011). We find that with $\alpha \sim 1$ and $\beta \sim 1$ reproduces the observed cloud velocities and the observed X-ray luminosity, where we have calculated the band-dependent X-ray emission from the wind using the same method as in Zhang et al. (2014). The value of β is consistent with Martin (2002). Using equation (21) we estimate the cloud flying distance $\Delta r \sim 20 - 30$ pc above the galaxy. We suggest that the spatial distribution and radial profile of acceleration of cool clouds could be used to further constrain the wind parameters in NGC 1569.

On the other hand, the hot wind parameters (α, β) for NGC 4449 required to yield clouds that reach $\sim 40 - 50$ km s⁻¹ produce too low X-ray emission and are inconsistent with observation. For example, the (very large) values of $\alpha \sim 1.0$ and $\beta \sim 1.0$ we calculate are needed to produce the cool cloud velocities, yield a hot and dense wind with an integrated X-ray luminosity of $L_X^{2-10 \text{ keV}} \sim 7.5 \times 10^{37}$ ergs s⁻¹, much lower than the upper limit to the diffuse X-ray emission observed ($L_X^{2-10 \text{ keV}} \simeq 1.4 \times 10^{39}$ ergs s⁻¹; Bogdán & Gilfanov 2011).

⁵ The timescale is from Scannapieco & Brügggen (2015) $t_{25} = 6 t_{\text{cc}}^{\text{th}}\sqrt{1 + \overline{M}_{\text{h}}}$, where t_{25} means that 25% of the cloud is below 2/3 of the initial cloud density.

Finally, due to the large gravitational potential in NGC 4214 with a value of $\sigma \sim 100 \text{ km s}^{-1}$ (Thronson et al. 1988; Schwartz & Martin 2004; D’Onghia & Lake 2008), clouds in NGC 4214 cannot be accelerated to the observed $V_c \sim 40 - 50 \text{ km s}^{-1}$.

In short, even though the observed cool cloud velocities are low in dwarf starbursts, we conclude that the CC85 model combined with RPA scenario can only explain some of them (e.g., NGC 1569). In addition, the spatial distribution and radial profile of acceleration of cool clouds, if observed, could be used to further constrain the wind parameters.

4.3 LIRGs and ULIRGs

Surveys of Na D absorption lines show cool gas outflows in LIRGs and ULIRGs with an average velocity at the line center of $300 - 400 \text{ km s}^{-1}$, and projected maximum velocities (average velocity at center plus one-half the velocity width) up to $\sim 1000 \text{ km s}^{-1}$.

We assume a fraction $f_d \lesssim 1$ of the observed total emission in X-rays from star-forming galaxies is due to a putative hot wind fluid, and then we ask whether such a flow can accelerate cool clouds to the observed velocities and physical scales. Because star-forming galaxies obey a mean linear $L_X - \text{SFR}$ relation, we take the relation from Mineo et al. (2014)

$$L_{X,\text{diffuse}}(0.5-8 \text{ keV}) = 4.0 \times 10^{39} f_d \text{ erg s}^{-1} \frac{\text{SFR}}{(M_\odot \text{ yr}^{-1})}. \quad (40)$$

Thus $f_d = 1$ is the observed mean relation between total X-ray emission and SFR. We assume that this fraction of the total band-dependent observed emission in equation (40) is due to the hot wind (Zhang et al. 2014):

$$L_{X,\text{hot}} = L_{X,\text{diffuse}}, \quad (41)$$

where $L_{X,\text{hot}}$ is the X-ray emission from the hot wind. Equation (41) is a function of (α, β) , R , SFR and f_d . If we combine equation (41) with the set of cloud acceleration equations (35), (36), and (37), the cloud velocity V_c can be calculated as a function of the SFR for a given parameter set of (α, β) , f_d , and cloud parameters r_0 , N_{H}^c and T_c . The relation between V_c and the SFR in the model can then be compared with the data from observations with the hope of constraining, ruling out, or providing evidence for the model.

We can calculate the maximum value of V_c (equations 35, 36 and 37) and SFR (equation 41) as functions of α , β , f_d , and R , and compare the calculated V_c -SFR relation with observations. Figure 6 gives examples of the fiducial model. Data on the maximum outflow velocities are taken from surveys of Na D or Mg II absorption lines (Heckman et al. 2000; Rupke et al. 2002; Schwartz & Martin 2004; Martin 2005; Rupke et al. 2005b,c; Weiner et al. 2009; Erb et al. 2012; Kornei et al. 2013). Since we do not know X-ray fluxes for all systems, we assume $f_d = 0.1$. As in our previous examples, we see that hot winds in LIRGs and ULIRGs cannot accelerate cool gas to the observed velocities in the Na D surveys for our fiducial parameters. Changing other parameters including T_c , r_0 , f_d and R does not change our results quantitatively. For example, assuming $f_d = 1$ or $R = 1 \text{ kpc}$, we find that V_c is always below $\sim 100 \text{ km s}^{-1}$. However, similar to our calculations for M82 in Section 4.1, larger κ (see Section 3.2) could mitigate this conclusion.

5 CONCLUSIONS

The cool gas with temperatures from $T_c \sim 10^2$ to 10^4 K seen in emission and absorption in galactic winds may be accelerated by the ram pressure of hot winds driven by overlapping supernovae (SNe) within rapidly star-forming galaxies. We have used analytic estimates and semi-analytic models to study the acceleration and destruction of cool gas clouds as a function of both hot wind and cool cloud properties. Our main conclusions are as follows.

(1) We find that over a very broad range of parameters cool clouds always establish pressure equilibrium with the hot flow before being accelerated (equations 15 & 16; Fig. 1).

(2) We derive a critical condition on the mass loading efficiency β (equation 2) such that clouds in pressure equilibrium are accelerated before destruction by the cloud shredding timescale (equation 19). For our fiducial assumptions about the timescale t_{sh} (equation 18), clouds with $T_c \lesssim 10^4 \text{ K}$ are destroyed before significant acceleration and these clouds do not reach velocities comparable to that of the hot wind (equations 19, 20, 21).

(3) We compare the gravitational force (F_{grav}) with the ram pressure force (F_{ram}), deriving an Eddington-like limit for $F_{\text{ram}} \geq F_{\text{grav}}$ as a function of cloud and host galaxy properties (equations 28, 32, 33; Fig. 2). If we take an initial cloud to be compressed by the ram pressure of the hot wind and come into pressure equilibrium with the hot wind, we show that the initial column density of launched clouds must be less than $\sim 10^{21} \text{ cm}^{-2}$ for outward acceleration with $T_c = 10^3 \text{ K}$ and $R = 200 \text{ pc}$ (equations 33, 34 and Fig. 2). Higher T_c or R can increase the upper bound to $N_{\text{H}} \lesssim 10^{22} \text{ cm}^{-2}$. These estimates depend sensitively on the properties of clouds.

(4) The timescale for cloud shredding t_{sh} plays the most important role in determining the final velocities of clouds V_c . For $T_c \sim 10^3 \text{ K}$, as might be appropriate for absorption studies of the Na D lines which have been widely observed in surveys of galactic outflows, V_c is limited to $\lesssim 100 \text{ km s}^{-1}$ by cloud shredding (equation 20; Figs. 3 and 4), and the clouds are accelerated and destroyed very near their starting positions r_0 (equation 21), potentially in conflict with observations. Similarly, warm clouds ($T_c \sim 10^4 \text{ K}$) and molecular clouds ($T_c \lesssim 100 \text{ K}$) cannot be accelerated by hot flows to observed velocities over virtually any range in parameter space. However, as we show in Section 3.2 (Fig. 5), V_c can be significantly higher if the magnetic cloud shredding timescale (t_{sh}) is increased by a factor of ~ 15 and ~ 5 for $T_c = 10^3 \text{ K}$ and 10^4 K respectively due to cloud magnetization (McCourt et al. 2015), as long as conductive evaporation can be neglected. We derive a critical κ_{crit} such that $t_{\text{sh}} \sim t_{\text{acc}}$ (equation 39) as a guide for current and future simulations.

We then compare our models with observations of outflows in M82, dwarf starbursts, LIRGs and ULIRGs. We combine the X-ray luminosities of star-forming galaxies with the scenario of ram pressure acceleration (RPA) of cool clouds by assuming a diffuse hot wind X-ray luminosity that contributes a fraction f_d to the total X-ray luminosity of star-forming galaxies (equation 40). As expected from our analytic investigation, this picture fails to produce velocities high enough to match observations, except for some dwarf starbursts (e.g., NGC 1569). However, as in our previous

examples, the cool clouds may well be explained if the cloud shredding time is much longer than implied by hydrodynamical simulations. Note, though, that even in cases where κ is 15 times larger and clouds reach large V_c , the spatial extend and the acceleration profile may be inconsistent with observations. The later thus provides a particularly powerful probe of the wind acceleration mechanism.

Overall we conclude that individual cool clouds with $T_c \lesssim 10^4$ K accelerated by ram pressure of a hot wind are not likely to match observed cool gas outflows. However, other cloud acceleration and formation scenarios or wind driving mechanisms may explain the observed properties of cool gas outflows in rapidly star-formation galaxies. In our model, we assume individual dense clouds with an initial scale of $\Delta R \sim N_{\text{H}}^1/2n_{\text{H}}^1 \simeq 0.2 \text{ pc } N_{\text{H},21}^1/n_{\text{H},3}^1$ and a mass of $M_c \simeq 0.4 M_{\odot} N_{\text{H},21}^{1,3} n_{\text{H},3}^{1,-2}$ to be accelerated in the hot wind. In reality, it may be that giant cool gas shells with masses of $\sim 10^8 - 10^{10} M_{\odot}$ on kpc scales are pushed out by the ram pressure of the hot wind, and that these shells eventually fragment, littering the hot outflow with cool gas clouds that are then accelerated on larger scales and mix with the hot wind. On the other hand, radiation pressure-driven winds may also be able to accelerate cool clouds (Murray et al. 2005; Krumholz & Thompson 2012, 2013; Hopkins et al. 2012; Zhang et al. 2014; Thompson et al. 2015). For example, in Zhang et al. (2014) we showed that radiation pressure driving is one possibility to explain the SFR- V_c relation observed in Na D surveys. Another possibility is that outflows are driven by the pressure of cosmic rays (e.g., Everett et al. 2008; Socrates et al. 2008; Jubelgas et al. 2008; Booth et al. 2013; Scannapieco & Brüggén 2015).

In summary, entrainment and ram pressure acceleration by a hot wind are strongly constrained. Clouds in only a narrow range of initial column densities can be accelerated, and are shredded rapidly at small distances from their launch radii and at relatively low velocities. This calls into question the prevailing picture where the gas probed by absorption and emission is thought to be entrained and ram pressure accelerated by the hot wind. Cool clouds can be accelerated to the observed velocities only if magnetic fields in the clouds are sufficiently important to prolong the lifetime of the clouds and suppress the evaporation, but even in this case the spatial extend and acceleration profile should be tested against observations of resolved systems like M82 (Section 4.1).

ACKNOWLEDGMENTS

We thank the referee Evan Scannapieco for his very useful comments that have allowed us to improve our paper. D.Z. thanks Crystal Martin, Sylvain Veilleux, Evan Scannapieco and Claude-André Faucher-Giguère, and T.A.T. thanks Tim Heckman for a number of stimulating discussions. E.Q. thanks Ryan O’Leary and Mike McCourt for useful conversations. This work is supported in part by NASA grant # NNX10AD01G. T.A.T is supported in part by NSF #1516967. E.Q. is supported in part by NASA ATP Grant 12-ATP12-0183, a Simons Investigator award from the Simons Foundation, the David and Lucile Packard Foundation, and the Thomas Alison Schneider Chair in Physics.

N.M. is supported in part by NSERC of Canada and by the Canada Research Chair program.

REFERENCES

- Aguirre, A.; Hernquist, L., Schaye, J., Katz, N., Weinberg, D. H., & Gardner, J. 2001, *ApJ*, 561, 521
- Alúzar, R., Pittard, J. M., Hartquist, T. W., Falle, S. A. E. G., & Langton, R. 2012, *MNRAS*, 425, 2212
- Chevalier, R. A., & Clegg, A. W. 1985, *Nature*, 317, 44
- Benson, A. J., Bower, R. G., Frenk, C. S., Lacey, C. G., Baugh, C. M., & Cole, S. 2003, *ApJ*, 599, 38
- Bogdán, Á. & Gilfanov, M. 2011, *MNRAS*, 418, 1901
- Bolatto, Alberto D., Warren, Steven R., Leroy, Adam K., et al. 2013, *Nature*, 499, 450
- Booth, C. M., Agertz, O., Kravtsov, A. V., & Gnedin, N. Y. 2013, *ApJL*, 777, 16
- Bower, R. G., Benson, A. J., & Crain, R. A. 2012, *MNRAS*, 422, 2816
- Brüggén, M., & Scannapieco, E. 2016, *ApJ*, 822, 31
- Cicone, C. et al. 2014, *A&A*, 562, 21
- Cooper, J. L., Bicknell, G. V., Sutherland, R. S., & Bland-Hawthorn, J. 2008, *ApJ*, 674, 157
- Cooper, J. L., Bicknell, G. V., Sutherland, R. S., & Bland-Hawthorn, J. 2009, *ApJ*, 703, 330
- Cowie, L. L. & McKee, C. F. 1977, *ApJ*, 211, 135
- Dekel, A., & Silk, J. 1986, *ApJ*, 303, 39
- D’Onghia, E., & Lake, G. 2008, *ApJL*, 686, 61
- Elbaz, D., et al. 2007 *A&A*, 468, 33
- Erb, D. K., Quider, A. M., Henry, A. L., & Martin, C. L. 2012, *ApJ*, 759, 26
- Everett, J. E., Zweibel, E. G., Benjamin, R. A., et al. 2008, *ApJ*, 674, 258
- Faucher-Giguère, C., Quataert, E., & Murray, N. 2012, *MNRAS*, 420, 1347
- Finlator, K., & Davé, R. 2008, *MNRAS*, 385, 2181
- Fischer, J., Sturm, E., González-Alfonso, E. et al. 2010, *A&A*, 518, 41
- Förster Schreiber, N. M., Genzel, R., Lutz, D., & Sternberg, A. 2003, *ApJ*, 599, 193
- Fujita, A., Martin, C. L., Mac Low, M.-M., et al. 2009, *ApJ*, 698, 693
- García-Burillo, S., Martín-Pintado, J., & Fuente, A., & Neri, R. 2001, *ApJ*, 563, 27L
- Grimes, J. P., Heckman, T., Strickland, D., & Ptak, A. 2005, *ApJ*, 628, 187
- Heckman, Timothy M., Armus, Lee, & Miley, G. K. 1990, *ApJS*, 74, 833
- Heckman, T., Lehnert, M. D., Strickland D. K., & Lee, A. 2000, *ApJS*, 129, 493
- Hopkins, P. F., Quataert, E., & Murray, N. 2012, *MNRAS*, 421, 3522
- Hunter, D. A., Rubin, V. C., Swaters, R. A., Sparke, L. S., & Levine, S. E. 2005, *ApJ*, 634, 281
- Huo, Z. Y., Xia, X. Y., Xue, S. J., Mao, S., & Deng, Z. G. 2004, *ApJ*, 611, 208
- Jun, B., Jones, T. W., & Norman, M. L. 1996, *ApJ*, 468, 59
- Jubelgas, M., Springel, V., Enlin, T., & Pfrommer, C. 2008, *A&A*, 481, 33

- Keeney, B. A., Stocke, J. T., Rosenberg, J. L., Tumlinson, J., & York, D. G. 2006, *AJ*, 132, 2496
- Kennicutt, R. C., Jr. 1998, *ARA&A*, 36, 189
- Klein, R. I., McKee, C. F., & Colella, P. 1994, *ApJ*, 420, 213
- Kornei, K. A., Shapley, A. E., Martin, C. L., Coil, A. L., Lotz, J. M., & Weiner, B. J. 2013, *ApJ*, 774, 50
- Krumholz, M. R., & Thompson, T. A. 2012, *ApJ*, 760, 155
- Krumholz, M. R., & Thompson, T. A. 2013, *MNRAS*, 434, 2329
- Krolik, J. H., McKee, C. F., & Tarter, C. B. 1981, *ApJ*, 249, 422
- Lehmer, B. D., Alexander, D. M., Bauer, F. E., et al. 2010, *ApJ*, 724, 559
- Lehnert, M. D., & Heckman, T. M. 1996, *ApJ*, 472, 546
- Leroy, A. K. et al. 2015, *ApJ*, 814, 83
- Mac Low, M., & McCray, R. 1988, *ApJ*, 324, 776
- Marlowe, A. T., Heckman, T. M., Wyse, R. F. G., & Schommer, R. 1995, *ApJ*, 438, 563
- Martin, C. L. 1998, *ApJ*, 506, 222
- Martin, C. L. 1999, *ApJ*, 513, 156
- Martin, C. L., Kobulnicky, H. A., Heckman, T. M. 2002, *ApJ*, 574, 663
- Martin, C. L. 2005, *ApJ*, 621, 227
- Martin, C. L. 2006, *ApJ*, 647, 222
- McKeith, C. D., Greve, A., Downes, D. & Prada, F. 1995, *A&A*, 293, 703
- Mellema, G., Kurk, J. D., & Röttgering, H. J. A. 2002, *A&A*, 395, 13
- McCourt, M., O’Leary, R. M., Madigan, A.-M., & Quataert, E. 2015, *MNRAS*, 449, 2
- Mineo, S., Gilfanov, M., & Sunyaev, R. 2012, *MNRAS*, 426, 1870
- Mineo, S., Gilfanov, M., Lehmer, B. D., Morrison, G. E., & Sunyaev, R. 2014, *MNRAS*, 437, 1698
- Murray, N., Quataert, E., & Thompson, T. A. 2005, *ApJ*, 618, 569
- Murray, N., Martin, C. L., Quataert, E., & Thompson, T. A. 2007, *ApJ*, 660, 211
- Nakamura, F., McKee, C. F., Klein, R. I., & Fisher, R. T. 2006, *ApJS*, 164, 477
- O’Connell, R. W., & Mangano, J. J. 1978, *ApJ*, 221, 62
- Oppenheimer, B. D., & Davé, R. 2006, *MNRAS*, 373, 1265
- Oppenheimer, B. D., & Davé, R. 2008, *MNRAS*, 387, 577
- Orlando, S., Bocchino, F., Reale, F., Peres, G., & Pagano, P. 2008, *ApJ*, 678, 274
- Ott, J., Walter, F., & Brinks, E. 2005, *MNRAS*, 358, 1453
- Panuzzo, P., et al. 2010, *A&A*, 518, 37
- Pasquali, A., et al. 2011, *AJ*, 141, 132
- Peeples, M. S., & Shankar, F. 2011, *MNRAS*, 417, 2962
- Pittard, J. M., Dyson, J. E., Falle, S. A. E. G., & Hartquist, T. W. 2005, *MNRAS*, 361, 1077
- Poludnenko, A. Y., Frank, A., & Blackman, E. G. 2002, *ApJ*, 576, 832
- Puchwein, E., & Springel, V. 2013, *MNRAS*, 428, 2966
- Rupke, D. S., Veilleux, S., & Sanders, D. B. 2002, *ApJ*, 570, 588
- Rupke, D. S., Veilleux, S., & Sanders, D. B. 2005, *ApJS*, 160, 87
- Rupke, David S., Veilleux, S., & Sanders, D. B. 2005, *ApJS*, 160, 115
- Rupke, D. S., Veilleux, S., & Sanders, D. B. 2005, *AJ*, 632, 751
- Sakamoto, K., Okumura, S. K., Ishizuki, S., & Scoville, N. Z. 1999, *ApJ*, 525, 691
- Sanders, D. B., Mazzarella, J. M., Kim, D.-C., Surace, J. A., & Soifer, B. T. 2003, *AJ*, 126, 1607
- Scannapieco, E., & Brüggem, M. 2015, *ApJ*, 805, 158
- Schiano, A. V. R., Christiansen, W. A., & Knerr, J. M. 1995, *ApJ*, 439, 237
- Schneider, E. E., & Robertson, B. E. 2017, *ApJ*, 834, 144
- Schure, K. M., Kosenko, D., Kaastra, J. S., Keppens, R., & Vink, J. 2009, *A&A*, 508, 751
- Schwartz, C. M., & Martin, C. L. 2004, *ApJ*, 610, 201
- Sharma, M., & Nath, B. B. 2012, *ApJ*, 750, 55
- Shopbell, P. L., & Bland-Hawthorn, J. 1998, *ApJ*, 493, 129
- Silich, S., Tenorio-Tagle, G., & Rodríguez-González, A. 2004, *ApJ*, 610, 226
- Silich, S., Tenorio-Tagle, G., & Muñoz-Tuñón, C. 2003, *ApJ*, 590, 791
- Socrates, A., Davis, S. W., & Ramirez-Ruiz, E. 2008, *ApJ*, 687, 202
- Stil, J. M., & Israel, F. P. 2002, *A&A*, 392, 473
- Strickland, D. K., & Heckman, T. M. 2009, *ApJ*, 697, 2030
- Strickland, D. K., Heckman, T. M., Colbert, E. J. M., Hoopes, C. G., & Weaver, K. A. 2004, *ApJ*, 606, 829
- Strickland, D. K., Heckman, T. M., Colbert, E. J. M., Hoopes, C. G., & Weaver, K. A. 2004, *ApJS*, 151, 193
- Strickland, D. K., Ponman, T. J., & Stevens, I. R. 1997, *A&A*, 320, 378
- Strickland, D. K., & Stevens, I. R. 2000, *MNRAS*, 314, 511
- Sturm, E., González-Alfonso, E., Veilleux, S., et al. 2011, *ApJ*, 733, 16
- Thompson, T. A., Quataert, E., Waxman, E., Murray, N., & Martin, C. L. 2006, *ApJ*, 645, 186
- Thompson, T. A., Fabian, A. C., Quataert, E., & Murray, Norman 2015, *MNRAS*, 449, 147
- Thompson, T. A., Quataert, E., Zhang, D., & Weinberg, D. H. 2016, *MNRAS*, 455, 1830
- Thronson, H. A., Jr., Hunter, D. A., Telesco, C. M., Decher, R., & Harper, D. A. 1987, *ApJ*, 317, 180
- Thronson, H. A., Jr., Greenhouse, M., Hunter, D. A., Telesco, C. M., & Harper, D. A. 1988, *ApJ*, 334, 605
- Veilleux, S., Cecil, G., & Bland-Hawthorn, J. 2005, *ARA&A*, 43, 769
- Veilleux, S., Rupke, D. S. N., & Swaters, R. 2009, *ApJ*, 700, 149L
- Vietri, M., Ferrara, A., & Miniati, F. 1997, *ApJ*, 483, 262
- Walter, F., Weiss, A., & Scoville, N. 2002, *ApJ*, 580, 21L
- Wang, B. 1995, *ApJ*, 444, 590
- Weiner, B. J., et al. 2009, *ApJ*, 692, 187
- Werk, J. K., Prochaska, J. X., Tumlinson, J., et al. 2014, *ApJ*, 792, 8
- Zhang, D., & Thompson, T. A. 2012, *MNRAS*, 424, 1170
- Zhang, D., Thompson, T. A., Murray, N., & Quataert, E. 2014, *ApJ*, 784, 93